Retrieval of O3 column densities at Islamabad, Pakistan by using ground-based MAX-DOAS

Hania Sabeen Minhas

(00000204786)

Institute of Environmental Sciences and Engineering,

School of Civil and Environmental Engineering,

National University of Sciences and Technology

Islamabad, Pakistan

(2020)

THESIS ACCEPTANCE CERTIFICATE

It is certified that the contents and forms of the thesis entitled **"Retrieval of O_3 column densities at Islamabad, Pakistan by using ground-based MAX-DOAS"** submitted by **Ms. Hania Sabeen Minhas,** Registration No. **00000204786** has been found satisfactory for the requirements of the degree of Master of Science in Environmental Science.

_____

Principal
Dr. Tariq Mahmood
SCEE, NUST

_____

Head of Department
Dr. M. Fahim Khokhar
Professor
IESE, SCEE, NUST

CERTIFICATE

It is certified that the contents and forms of the thesis entitled **"Retrieval of O_3 column densities at Islamabad, Pakistan by using ground-based MAX-DOAS"** submitted by Ms. Hania Sabeen Minhas have been found satisfactory for the requirements of the degree of Master of Science in Environmental Science.

Supervisor: _____

Dr. M. Fahim Khokhar

Professor

IESE, SCEE, NUST

Member:

_____

Dr. M. Zeeshan Ali Khan

Assistant Professor

IESE-SCEE, NUST

Member:

_____

Dr. Sher Jamal Khan

Professor

IESE-SCEE, NUST


بسم الله الرحمن الرحيم

ACKNOWLEDGEMENT

In the name of Allah, the Most Gracious and the Most Merciful. Alhamdulillah, all praises to Allah for granting his blessing and strength in completing this thesis.

I would like to express sincere thanks to my supervisor **Professor Dr. M. Fahim Khokhar**, whose keen interest, suggestions and guidance were invaluable and remained helpful throughout my research work. His incredible guidance, sustained encouragement and sympathetic attitude during the period of my research enabled me to technically tackle all the problems during the course of study. The illustrious advices, valuable suggestions and inspiring attitude of **Dr. Zeeshan Ali Khan** and **Dr. Sher Jamal Khan** made it very easy for me to undertake this work throughout the course of this research work.

This acknowledgement would be incomplete if I do not pay my sincere and heartfelt thanks to my cherished and loving parents for their sacrifices, prayers, and affections without which it would have been just a dream to achieve any goal. My sincerest thanks to all my friends for their continuous support and encouragement throughout the research phase. Last but not the least I would like to thank all the laboratory staff at IESE for their help and cooperation.

Hania Sabeen Minhas

Abstract

Air pollution is among the leading environmental and human health issues around the globe, especially for developing countries like Pakistan. According to recent reports from WHO, all cities under study exceed Pak-NEQs for Ambient Air. Among various atmospheric pollutants, tropospheric ozone is one of the criteria pollutants responsible for the formation of photochemical smog and various human health impacts. In this study, ground based MAX-DOAS monitoring performed at NUST, Sector H-12, Islamabad, Pakistan is used to retrieve tropospheric ozone concentrations for the time period of March 2015 - March 2019. Average diurnal variation of tropospheric ozone at the study site exhibited minimum during early morning i.e. 6 am - 6:59 am when traffic load is low and sunlight is weak. Consequently, maximum values are reached around noon and during peak traffic hours. Average monthly variation of tropospheric ozone showed an increasing trend from the March to July, where after ozone pollution subsides significantly during the colder months.

Results show a direct relation between temperature and tropospheric ozone column densities with Pearson value (r=0.58). Similarly, Global Horizontal Irradiance and Tropospheric ozone column densities were also investigated and exhibited a Pearson value (r=0.56). MAX-DOAS observations were validated against satellite observations from the combined product of MLS/OMI instruments, exhibiting a positive correlation (r=0.80). MAX-DOAS observations of tropospheric ozone levels are well within the WHO standards for most days of the study period.

CHAPTER 1

INTRODUCTION

1.1 Background

Air pollution ranks among the major health and environmental issues globally, caused primarily by anthropogenic activities such as fossil fuel burning in industries and traffic. Recent decades have seen exponential rise in human health impacts caused by air pollution. Studies have established the link between air pollution and rise in morbidity and mortality due to cardiovascular and respiratory diseases, as well as the occurrence and progression of serious health issues such as Alzheimer's and Parkinson's diseases, autism, retinopathy, retarded fetal growth, and low birth weight.

The industrial revolution fed on coal and other fossil fuels, leading to the devastating environmental and health impacts like in the case of the London Smog during December 1952, claiming 4000 lives in 4 days. Later epidemiology studies reported that the long-term consequences of the smog episode took the death toll up to 12000 people. Increasing industrialization, population rise and urbanization are the major reasons behind ever-worsening air pollution today. Countries across the world have devised standards and guidelines to curb air pollution, in addition to signing international agreements to keep global pollution levels below certain limits in order to safeguard human health and the environment.

1.2 Ozone (O_3)

Ozone is one of the most important atmospheric trace gases in the stratosphere and the troposphere. 90% of earth's ozone is concentrated in the ozone layer situated in the stratosphere, shielding the surface from the sun's harmful UV radiations. The remaining 10%, termed tropospheric ozone, is one of the criteria pollutants that reside in the troposphere and has adverse impacts on human health and vegetation. Generated mainly from anthropogenic sources, it is the 3rd largest contributor to the total tropospheric radiative forcing, with a radiative forcing of 0.40 ±0.20Wm^{-2}.

High ozone concentrations (estimated 220 ppb) were first recorded during the Los Angeles (photochemical) smog incident of 1952, characterized by low visibility, crop damage, eye irritation, objectionable odor and deterioration of rubber. Tropospheric ozone is termed by many as the most damaging air pollutant to vegetation, with impacts including visible leaf injury, in specie composition and reduction in forest growth.

Tropospheric ozone also contributes significantly to deterioration of built infrastructure exposed to the outside air, including steel, stone, concrete, brick and wood. Based on its impacts, ozone was declared one of the "Criteria Pollutants" by the 1970 Clean Air Act alongside gases such as sulfur dioxide, the cause of sulfurous smog.

Being the fourth major contributor towards global warming after water vapor, CO_2 and CH_4, increase in tropospheric ozone requires immediate attention. While ozone level reductions are being achieved in most developed nations, increasing trends are being observed over most locations in Asia, including the Indian region, where the impacts of ozone are largely unknown. Ozone-related deaths are estimated to make up about 5–20 %

of all air pollution related deaths at present, roughly 470,000 premature respiratory deaths globally and annually.

Though ozone is a relatively short-lived pollutant, with lifetime of typically hours, in polluted urban regions where ozone precursors are present around the clock in high concentrations, its lifetime in troposphere extends up to several weeks. Intercontinental transport of ozone influences air quality on a hemispheric scale and impacts remote rural settlements as well as forests. Transport of tropospheric ozone from polluted regions upwards to pristine high altitude regions as well as downwards to un-polluted marine regions has been documented, changing regional ozone budgets. Ground-level ozone concentrations at all the major and minor urban centers must be monitored, and the impacts of various factors such as temperature and wind on its concentration and trends must be studied.

1.3 The Instrument: MAX-DOAS

Multi-Axis Differential Optical Absorption Spectroscopy (MAX-DOAS) is a passive remote sensing technique for measuring tropospheric aerosol load and trace gas concentrations and generating spatial and temporal records. The instrument works on the principle of “Lambert Beer Law”. MAX-DOAS determines the amount of light absorbed by various gases in various wavelength ranges to determine their concentrations along the path of sunlight absorbed by the spectrometer

The DOAS method is applied to the recorded spectra of scattered sunlight at different viewing angles α (angle b/w horizon and telescope direction) to generate Slant Colum Densities (SCDs) of aerosols and trace gases, The measured SCDs represent ozone

molecules present in the light's path, from near sources as well as molecules carried by wind currents across thousands of miles. Wind direction and wind speed data may be used to generate accurate flux data for the individual gases to determine their sources and major contributors.

1.4 Pakistan National Environmental Quality Standards

Pakistan Environmental Protection Agency has formulated standards for all the major air pollutants (table 1) to curtail the levels of air pollution in the country. Industries are regulated by these National Environmental Quality Standards (NEQs) for ambient air.

1.5 World Health Organization Air quality guidelines

The World Health Organization sets the standards for 8-hour averaged concentration of ozone in ambient atmosphere. As the Pak-EPA does not provide a standard for 8-hour average or daily average value of ozone, WHO air quality guidelines will be used for this study to determine the extent to which the measured values comply with the safe levels set by WHO.

1.6 Objectives

The study was designed to achieve the following objectives:

1) To monitor ground level concentration of tropospheric O_3 at IESE, NUST, Sector H-12 Islamabad, Pakistan.
2) To validate the MAX-DOAS measurements using the combined product of MLS/OMI instruments.

CHAPTER 2

LITERATURE REVIEW

2.1 The Earth's Atmosphere

Atmosphere is defined as the gaseous envelope around the earth, responsible for sustaining life by providing the air we breathe, driving the currents that regulate climate and absorbing the harmful UV radiations coming from the sun. It is a mixture of various gases present in specific concentrations to make it life sustaining for living organisms.

2.2 Structure of the Atmosphere

The earth's atmosphere is divided into five layers: the troposphere that we live in near the surface of the earth; the stratosphere that houses the ozone layer; the mesosphere, a colder and lower density layer with about 0.1% of the atmosphere; the thermosphere, the top layer, with high temperatures and low molecular density, and the exosphere, the actual "final frontier" of Earth's gaseous envelope. Separating these layers are the three transitional layers: the tropopause between troposphere and stratosphere; the stratopause between stratosphere and mesosphere and the mesopause between mesosphere and thermosphere.

2.2.1 Troposphere

It is the lowest layer of the atmosphere extending from the surface up to 16-18 km at the equator and 7-8 km at the poles. The variation occurs due to earth's rotation which tends to shift air masses towards the equator. As height increases in troposphere, pressure drops and temperature decreases at the 'lapse rate' of 6.5°C/km, reaching as low as -60°C at the top of the troposphere. Most of what we call atmosphere is present in the troposphere, and nearly all weather occurs in this layer.

2.2.2 Stratosphere

The layer above troposphere and separated from it by the tropopause is known as the stratosphere and extends up to 50 km. It contains 15% of the atmosphere's total mass even though no weather exists here, making it the second major layer. The reason behind the calm conditions is the trend of increase in temperature (produced during ozone formation) with altitude, preventing updrafts of the troposphere beneath and effectively preventing turbulence and weather of all kinds. Commercial passenger jets fly in the stratosphere due to lack of turbulence.

- **Ozone layer**

The defining feature of stratosphere is the presence of the ozone layer or ozone shield, a region containing high concentration of ozone molecules (approx. 10 parts per million) as compared to other parts of the atmosphere (0.3 parts per million). Found between 15 to 35 kilometers above surface, its thickness varies with location and season. Ozone layer is of enormous importance to all life forms on earth as it absorbs 97 to 99 percent of all the low wavelength ultraviolet radiation entering the earth's atmosphere from the sun, protecting us from the health impacts of UV exposure such as cancer, eye and skin diseases.

2.2.3 Mesosphere

The layer above stratosphere, known as the mesosphere extends up to 80km above surface. Separated from the stratosphere by the boundary layer stratopause, the temperature grows colder as height increases through the mesosphere, reaching -90° C at the top of the layer. This layer protects the earth from meteors and asteroids that enter the atmosphere by burning them due to friction caused by incredibly low temperature and pressure.

2.2.4 Thermosphere

The layer above mesosphere, known as the thermosphere extends up to 600 km, however variations in the amount of incoming solar radiation can raise this layer to 1000 km. Separated from the mesosphere by the mesopause, temperature in this layer shows an increasing trend with rising altitude as high-energy X-rays and UV radiation from the Sun are absorbed. Thermosphere is responsible for telecommunication on earth, with most satellites orbiting the earth in this region. The aurora, the Northern Lights and Southern Lights, occur in the thermosphere.

2.2.5 Exosphere

Starting at the top of the thermosphere at about 1000km, exosphere extends to somewhere between 100,000 km and 190,000 km, the latter being half the distance to the Moon. Exosphere is more space-like than the thermosphere, with extremely thin air that is gradually but steadily leaking out of the Earth's atmosphere into outer space.

2.3 Stratospheric Ozone

90% of earth's ozone budget is present in the lower portion of the stratosphere, in a region between 15 and 35 **kilometers** above surface, known as the ozone layer. High frequency UV radiations from the sun break down oxygen molecules into highly reactive atomic oxygen, which in turn bind with stable diatomic oxygen molecules to produce ozone molecules.

The continuous production of stratospheric ozone is balanced by its destruction as it reacts continually with sunlight and a wide variety of natural and anthropogenic chemicals such as hydrogen and nitrogen oxides, chloro and bromo compounds. These reactions convert

UV radiation into thermal energy, raising the temperature of the stratosphere. The entire cycle of ozone creation and destruction, and the net conversion of UV radiation into thermal energy is termed as the Chapman Cycle.

2.4 Tropospheric Ozone

The remaining portion of the earth's ozone budget (10%) is present in the troposphere. Ground level ozone reactions also require sunlight for ozone creation and destruction. In unpolluted atmosphere, the two processes create a net balance, but due to increase in precursor pollutants (primarily due to fossil fuel combustion), the net result in recent decades has been a steady rise in tropospheric ozone across the globe. Figure 6 depicts the production of ground-level ozone through the reactions between precursor pollutants in the presence of sunlight.

Ozone has a very short global mean lifetime in the troposphere (~3 weeks) compared to other long-lived species, with sources and sinks that vary greatly across temporal and spatial scales. Due to its shorter lifetime and varied sources, it is also not mixed well, resulting in large spatial and temporal variations over seasonal, annual and decadal timescales. These varied trends are further reinforced by its strong dependence on sunlight and precursor emissions, which have both natural and anthropogenic sources that can vary greatly across time and space.

Understanding tropospheric ozone chemistry is essential as it is a powerful greenhouse gas and a precursor for the highly reactive hydroxyl radical, which determines the chemical composition of the troposphere.

2.4.1 Physical and Chemical Properties of Ozone

Ozone, also known as tri-oxygen, is a pale blue gas with a distinct pungent odor, detectable at concentrations as low as 100 ppb in air. Ozone is an unstable allotrope of oxygen, prone to decompose explosively when heated rapidly to the boiling point. Ozone is a powerful oxidant and is used commercially in processes such as:

- Production of pharmaceuticals, synthetic lubricants and other organic compounds.
- Disinfecting municipal water supplies as it kills bacteria but does not produce organochlorine compounds like chlorine water treatment.
- Decontaminating operating rooms between surgeries, and hospital laundry.
- Used in grain silos to kill insects in stored grain and in food processing industries (scrubs yeast and mold spores from air).
- Used as a flocculation agent (agglomeration and settling of harmful molecules such as iron, arsenic and nitrates).
- Determining the age of rubber samples to find out the useful life of a batch of rubber.
- Eradication of water-borne parasites in water treatment plants.
- Detoxifying cyanide wastes produced in gold and silver mining by oxidizing cyanide to cyanate and eventually to carbon dioxide.

2.4.2 Precursors of Tropospheric Ozone

Photo-oxidation of CH_4, CO, Non-methane hydrocarbons (NMHCs) and volatile organic compounds (VOCs) in the presence of sufficient amount of NO_x in the air and sunlight

result in the production of ozone. NOx is the limiting factor in the production of tropospheric ozone, controlling its production and destruction. The major portion of precursor emissions are generated from anthropogenic sources such as vehicular emissions and industrial emissions, however natural emissions of precursor compounds also play a significant role in regulating ozone concentrations, especially in rural areas where anthropogenic sources are largely absent. Some natural sources of ozone precursors include: soil NO_x emissions, lightning NO_x emissions, biogenic VOC (BVOC) emissions, wildfire emissions and wetland methane emissions.

Soil NO_x Emissions

Microbial activity in soil accounts for 10-15% of all global NO_x emissions. It is dependent on the availability of inorganic nitrogen, type of vegetation and climatic conditions such as temperature and moisture. Soil NO_x emissions increase exponentially with soil temperature until 30°C, above which water becomes the limiting factor. High soil moisture reduces oxygen in the soil, increasing de-nitrification and reducing NO_x production.

Daily NO_2 observations made by OMI satellite during the summer monsoon season in three remote rural locations in India recorded rapid and intense bursts of NO_x emissions, caused by sudden shifts from dry to wet conditions. Bursts of NO_x emissions were also observed through SCIAMACHY observations in the USA.

Lightning NO_x Emissions

Energy produced by lightning flashes accounts for an approximate 2 to 8 Tg N/yr. Lightning NO_x emissions make a significant contribution (10ppbv) to the upper

tropospheric ozone where ozone production is most efficient, and ozone has longer lifetime.

Model projections over 169 Chinese cities in 2016 and 2017 were made using the GEOS-Chem chemical transport model to discover contributions of anthropogenic, background and individual natural sources to surface ozone. Large contributions from natural sources (80% in March-April and 72% in May-August) were discovered.

Biogenic VOC Emissions

Biogenic VOCs are important ozone precursors, generated during photosynthesis and vary greatly across plant species. Field and laboratory observations show exponential rise in biogenic isoprene and monoterpene emissions with rising temperature, determining temperature as the limiting factor. The exponential rise of BVOC emissions with temperature also drives the positive ozone-temperature correlation found over urban areas where NO_x levels are high.

Wildfire Emissions

Wildfires release large amounts of ozone precursor gases (CO, NO_x and VOCs) and produce roughly 3.5% of the total ozone produced annually. Combustion efficiency plays a significant role in determining the secondary emissions from a wildfire event. Flaming combustions resulting from high temperatures cause stronger oxidation of fuel nitrogen compounds, leading to higher NO_x emissions and ultimately higher ozone production. Smoldering wildfires however cause ozone enhancement downwind as the low

temperatures convert NO_x to PAN which can travel significant distances away from the burning sites.

2.5 Seasonal Variability of Tropospheric Ozone

Surface measurements of ozone over Ahmedabad (233°N, 72.63°E) in tropical India during 1991-1995 showed high levels of ozone (ppb) during autumn and winter. The rise was attributed to high precursor levels caused by large scale inter-continental transportation and lower boundary layer heights during cold months.

Investigation into the climatology and long-term trends of tropospheric ozone over South Asia during 2005-2017 period discovered elevated tropospheric ozone loading (~50 DU) along the Indo-Gangetic Plain (IGP) during pre-monsoon and summer monsoon seasons, also revealing strong inter-annual variations of 10-15 DU. Year-round increase in the Tropospheric Column Ozone (TCO) was observed across the South Asia region. Wintertime TCO showed a 3% yearly increase over the western India and Northwest Indo-Gangetic Plain (IGP), corresponding to rise in anthropogenic emission in the region.

Seasonal variability of various pollutant gases over South Asia is of particular importance to the global atmospheric composition, due to tropical convection combined with strong horizontal winds in this region, especially in the Upper Troposphere and Lower Stratosphere (UTLS). The seasonal variability of tropospheric ozone is impacted by various factors such as cloud chemistry, the monsoon system and climate change.

2.5.1 Impacts of Cloud Chemistry on Tropospheric Ozone

Clouds strongly impact the photochemical processes in the lower half of the troposphere. Water vapor saturation in the air prevents penetration of reaction-initiating sunlight.

Aqueous-phase processes reduce the gas-phase concentration of pre-cursor chemicals and produce ozone-depleting compounds. Formaldehyde (CH_2O) is a major intermediate gas in the oxidation of various hydrocarbons (e.g. ethene, isoprene, and methane) released by forests, biomass burning, traffic and industrial processes. CH_2O breaks down at an accelerated rate in the aqueous phase, creating oxidation products which react with ozone, acting as a significant sink. Furthermore, cloud processing of nitrates depletes NO_2, the limiting factor for production of tropospheric ozone.

2.5.2 Impacts of Monsoon on Tropospheric Ozone

The onset of summer monsoon causes decline in tropospheric ozone over southeast Asia from May to August, observed through satellite and ground observations. Cleaner marine air input and stronger air uplift during the wet monsoon and the cloudy, cool and wet weather conditions cause drop in ozone chemical production.

Quantification of constituent processes across the Indian lower troposphere from May to August showed a 4.2 Tg decrease in chemical ozone production and uplifting of 3.3 Tg ozone (due to strong convection); leading to significant decreases in the Indian lower tropospheric ozone during the monsoon months. The uplifted ozone is transported by the easterly jet in the upper troposphere to the rest of the globe, impacting global tropospheric ozone distribution. Differences in strength of the monsoon system can cause variations of as much as 3.4 ppbv.

2.5.3 Impacts of Climate Change on Tropospheric Ozone:

Global and regional tropospheric ozone levels respond significantly to meteorological conditions and changes in climate. Future climate change is projected to increase ground-

level ozone in polluted regions and cause a decrease at the global scale due to stronger chemical losses. These changes can be modelled and explained through three different pathways of climatic impacts on tropospheric ozone. These pathways are:

1. Impacts of climate change on precursor emissions from natural sources.
2. Impacts of climate change on chemistry and deposition of ozone and its precursor compounds.
3. Impacts of climate change on transport patterns of ozone and its precursor compounds.

Impacts of climate change on Precursor Emissions

The natural sources of ozone precursors; soil NO_x emissions, lightning NO_x emissions, biogenic VOC (BVOC) emissions, wildfire emissions and wetland methane emissions are impacted significantly by changing meteorological conditions brought on by climate change.

Soil NO_x emissions are projected to trigger strong local ozone production in rural areas where NO_x is the limiting factor, accounting for nearly half of the increased ozone in rural Southeastern U.S. An increase of 25% in NO_x emissions and 2 ppbv in surface ozone were simulated over the industrial eastern China, as a result of warmer climate. Models project significant rise in soil NO_x emissions (23% higher by 2100), resulting in increased ozone production.

A 3°K rise in temperature increases biogenic isoprene emissions by 6-31%, in turn increasing surface ozone by more than 2 ppbv in northern mid-latitudes. The enhanced

isoprene levels also lead to the production of more peroxyacetyl nitrate, PAN (a NO_x reservoir compound), which can travel long distances and produce ozone downwind. Models project significant rise in BVOC emissions as the result of global warming, resulting in higher tropospheric ozone concentrations.

Rising temperatures and dry weather conditions due to global warming have been conclusively linked with increase in intensity and frequency of wildfires in the western US since 1970. Large wildfire events occur more frequently with rise in temperature and solar radiation, and with decreasing humidity and wind speed, with four times as many large wildfire events as small wildfire events at temperatures above 30°C.

Impacts of climate change on chemistry and deposition of ozone and its precursor compounds

Meteorology impacts tropospheric ozone production by regulating the efficiency of deposition of various precursor and intermediate substances such as PAN (Peroxyacetyl Nitrate), HO_x (water vapor) and dry deposition of tropospheric ozone.

PAN is generated through the oxidation of acetaldehyde in hydrocarbon-rich environment using NO_x as a catalyst. The formation process of PAN serves as sink for both NO_x and peroxy radicals, reducing ozone production in and around the region. It acts as a NO_x reservoir compound, traveling across the colder higher troposphere, transporting NO_x from highly polluted regions and fire spots to remote regions where it reacts with other precursors in the presence of sunlight to produce ozone. Rising global temperatures are projected to cause rapid PAN decomposition, increasing ozone production in polluted

regions and reducing it in remote regions as transport of PAN (through colder higher troposphere) will no longer be dominant.

Dry deposition on vegetation acts as a sink for 20% of total annual tropospheric ozone. Dry deposition occurs mostly through stomatal uptake on leaf surfaces and is dependent on climatic factors such as light, temperature, soil moisture and humidity. Adverse weather conditions such as drought and high air or soil temperatures suppress stomatal uptake to protect against desiccation, increasing ozone levels in semi-arid regions as well as high latitude regions on hot dry days. The remaining portion of dry deposition is attributed to non-stomatal ozone deposition i.e. the thermal decomposition of ozone with external surfaces including soil and canopy, and is also dependent on temperature and solar radiation. Projections of future surface ozone over Europe using chemistry transport models (CTMs) have predicted increased ozone dry deposition during winter due to reduced snow cover, whereas in summer, changes in soil moisture, temperature and air stability will suppress ozone dry deposition, leading to a 6 ppbv rise in ozone over Europe. The relatively weaker process of dry deposition accounts for more than 60% of the total ozone enhancements, making it a key player in climate-induced future ozone changes.

Impacts of climate change on Transport Patterns of Ozone and its precursors

Due to lifetimes reaching several weeks up to months, ozone and its precursors compounds travel across large distances from polluted regions to pristine areas where little to no anthropogenic emissions are present. Weather patterns responsible for trans-boundary and trans-continental transport of pollutants can be classified into three categories based on

their spatial scales. These are; synoptic circulations (~1000 km), large-scale climate patterns (~10,000 km), and global vertical circulations.

Stratosphere-Troposphere Exchange, driven by large-scale stratospheric meridional circulation known as the Brewer-Dobson circulation accounts for approximately 10% of the annual global tropospheric ozone chemical production. Brewer-Dobson circulation has been strengthening in the recent decades and is expected to get stronger as global warming progresses. Future climate change is projected to increase STE by 17% and 28% (acc. to two different model projections) in 2100 compared to 2000, raising tropospheric ozone levels. Positive tropospheric ozone trends at various sites have been reported and linked to stronger STE caused by global warming events.

2.6 Tropospheric Ozone as an Oxidizing Agent

Ozone is a very strong oxidizing agent, contributing enormously to the oxidative capacity of the atmosphere. Ozone plays a major role in atmospheric chemistry by dominating the formation of hydroxyl radical, which in turn impacts the lifetimes of various trace gases such as methane and hydro-chlorofluorocarbons (HCFC). The biological effect of ozone is attributed to its stability to cause oxidation of biomolecules, directly as well as through various free radical reactions. It is the major constituent of photochemical smog and causes various health impacts in plants and humans, resulting in its status as one of the criteria air pollutants.

2.6.1 Impacts on humans

The oxidative potential of ozone initiates various reactions in human body, including lipid peroxidation and loss of functional groups of enzymes, alteration of membrane

permeability, and cell injury or death. The most pervasive impacts are in the form of various lung injuries. The most evident proof of damage is seen as loss of cells and accumulation of inflammatory cells at the junction of terminal bronchioles and alveolar ducts. The human body rebounds from short-term exposure through the initiation of a recovery phase, where cell damage and loss of enzyme activity during exposure is followed by increased metabolic activities, coinciding with a proliferation of metabolically active cells. Chronic exposure to ozone on the other hand can exacerbate lung diseases and increase the chances of lung tumor in susceptible populations. Besides the impacts on lungs, extra-pulmonary effects involving the blood, spleen, central nervous system, and other organs have also been observed. O_3 may also act in synergy with other air pollutants in photochemical smog such as NO_2 to produce enhanced effects. The major pathway of resistance against ozone poisoning is increase in uptake of dietary antioxidants such as vitamin E, vitamin C, and selenium.

2.6.2 Impacts on vegetation

Tropospheric O_3 is highly phytotoxic, causing both acute (symptomatic) and chronic (changes in growth, yield or productivity and quality) impacts, the latter being an increasingly prevalent problem in both crops and forests. Tropospheric ozone reduces vegetative productivity. As the precursors of ozone, NO_2 and VOCs are also generated from natural sources such as lightning and specialized vegetation, the problem of ozone is not limited to cities or polluted places. Ozone has been recognized as the most important rural air pollutant, affecting human health as well as vegetation of all kinds. Concentration of O_3 in the air and stomatal conductance determine the rate of O_3 uptake.

2.7 DOAS Spectroscopic Method

DOAS is one of the most extensively used spectroscopic techniques in atmospheric research. It is used to classify the column densities of different trace gases in the atmosphere. Introduced by Platt and his companion in 1979, the technique is based on the absorption of different wavelengths of light (in Ultra-Violet and Visible range) by different species. DOAS can measure various trace gases such as SO_2, NO_2, BrO, O_3, HCHO and CHOCHO. Figure 5 shows the components of a simplified DOAS setup.

Multiple gas column densities can be retrieved simultaneously using DOAS, saving time and allowing accurate comparisons of different gases in the observed air mass. DOAS techniques can be broadly classified into two types: active DOAS measurement techniques using artificial light sources and passive DOAS measurement techniques using natural light i.e. sunlight. The working principal of DOAS technique is based on "Lambert beer Law", which states the linear relationship between light and matter. According to this law, absorption of light is directly proportional to its path length and concentration of the analyte.

The comparison of incoming radiation ($I_{O\lambda}$) with outgoing (I_λ) by a function of path length (L) of the light and the concentration (c) and absorption cross-section (σ_λ) of the species is given in the equation:

$$I_\lambda = I_{0\,\lambda} . e^{-L\sigma(\lambda) c}$$

This relationship can be used to calculate the column densities of a trace gas by setting up a light source of known spectral intensity and a sensor at some distance (L). The working principle is given in figure 6.

2.7.1 Satellite Observation: OMI

Ozone Monitoring Instrument (OMI) has a high spectral resolution and has the ability to measure several trace gases in the UV/Vis wavelength range for a given air mass. The spectral range in which reflected light is observed by Ozone Monitoring Instrument (OMI) is usually between Ultra-violet to Visible (i.e. 270nm–500nm) with a spectral resolution of 0.5nm. The Ultra-Violet Channel is further divided into two sub channels UV-1 (270-310nm) and UV-2 (310-365nm).

Chapter 3

MATERIALS AND METHOD

3.1 Instrument: Mini MAX-DOAS

The Multi Axis-Differential Optical Absorption Spectroscopy (MAX-DOAS) is a highly sophisticated lightweight device that can be used for both stationary and mobile monitoring of trace gases. It is specially designed to monitor backscattered sunlight. Optical Fiber cable spectrograph and other controlling electronic parts are tightly closed in an aluminum box. A stepper motor is used to move the instrument at different elevation angles (Precision = 0.1 degree/step, Frequency= 784Hz). A quartz lens with a focal length of 40mm is used to focus light on the spectrometer. The spectral range is detected by a “Czerny Turner Spectrometer (Ocean Optics Inc., USB-2000+). For continuous ground-based monitoring and periodic field measurements, the detectable range of spectrometer is 305-440 nm and the spectral resolution is 0.7nm. The device has a resolution of 2048 pixels and uses Peltier cooling (Thermoelectric cooling) to regulate its temperature. DOASIS (Differential Optical Absorption Spectroscopy Intelligence System) operational algorithm is run on the connected computer to regulate the device and store recorded spectra.

3.1.1 Monitoring Site

The MAX-DOAS instrument used in the study is installed at the roof of the Institute of Environmental Sciences and Engineering (IESE) NUST. Continuous monitoring was carried out during daylight hours from March 2015 to March 2019. Table 3 enlists the software used during the course of this research.

3.1.2 DOASIS

DOAS intelligent system is the software used to operate the MAX-DOAS instrument. DOASIS is vital for data retrieval, rotating the instrument at different elevation angles, regulating the temperature of the instrument and setting spectrum integration time. The software runs on java coded script which provides all the necessary commands. To calibrate the instrument, dark current and offset were taken manually and automatically as coded in the script. The DOASIS software was also used to calculate the ring spectrum. Both ring spectrum and OSDC (Offset Dark current) are used during the analysis of data in QDOAS. Figure 7 shows the DOAS Intelligent system software interface.

Dark Current: This small electric current is normally measured in the photosensitive instrument (e.g., Spectrometer). For dark current monitoring a long exposure time and a smaller number of scans is required.

Off Set: The offset is taken in completely dark conditions, in other words "in the absence of photons". For offset measurement, a small exposure time and a greater number of scans are required.

3.2 Retrieval of O_3

The three analysis steps used to retrieve trace gas measurements from MAX-DOAS:

i. Wavelength Calibration
ii. Wavelength Convolution
iii. O_3 Analysis Window

3.2.1 Wavelength Calibration

For wavelength calibration, WinDOAS (Windows Differential optical absorption spectroscopy) is used. Spectrum recorded at 90^o angle at noon time with the lowest recorded SZA is used to calibrate the instrument. The calibration fit is also known as "Kurucz-fit" and is further convoluted as per the spatial resolution of the mini MAX-DOAS instrument. The wavelength range is divided into several sub-windows (sub-windows = 6) for analyzing the fits in each sub-window. For adjustment of spectrum shift between convoluted and measured spectra, "shift and squeeze" is applied. All measured spectra are evaluated using the calibration file against a reference spectrum. The Calibration Window of WinDOAS is shown in figure 8.

3.2.2 Wavelength Convolution

Convolution is a mathematic method used in wavelength processing operations. In QDOAS software "convolution tool" is used to execute the convolution. There are two types of convolution.

Online Convolution: In online convolution, cross sections are automatically convoluted during analysis without any pre-processing, by simply inserting them in the trace gas analysis window.

Offline Convolution: In offline convolution, the cross sections are convoluted before inserting them in the trace gas analysis windows. In this study, online convolution of cross sections is employed.

3.2.3 Cross Sections and O_3 Analysis Window

The cross sections of different trace gases used in the convolution process with their convolution specifications, and analysis windows for O_3 analysis are listed in table 5. "Standard convolution" (Convolve Std) tool is used to convolute the cross-sections with the highest resolution. Slit function type Gaussian (FWHM = 0.7nm) and standard calibration are used. "I_0 correction" (Convolve I_0) tool is used to evaluate the optical depth in convolution.

3.3 QDOAS Analysis settings

Various parameters are set in the QDOAS software before the addition of cross-sections. Some of these parameters have been determined by previous studies on the instrument and are duplicated for this study. These include: Display Settings and Instrumental settings.

3.3.1 Display settings

Figure 9 shows the four display fields selected for analysis i.e. for each spectrum, the four parameters will be available for comparison and trend analysis. These are: date, time, Solar Zenith Angle and Elevation Viewing Angle.

3.3.2 Instrumental Settings

Figure 10 shows the various instrumental settings employed for QDOAS analysis.

Detector size: 2048, determined by the make of the instrument

Calibration: The calibration file generated using WinDOAS is added for analysis

Dark Current and Offset: DC and OS files are generated manually each day on the DOASIS software and used with the corresponding spectra for accurate retrieval.

3.4 Sensitive Case Study

A Sensitive case study was carried out to quantify the impacts of variations in several parameters on the RMS, SCDs error, total analysis error and the level of uncertainty in each analysis. These parameters were: Polynomial order, fitting interval and cross-sections. Study conducted titled: "Vertical Profiles of Tropospheric Ozone from MAX-DOAS Measurements during the CINDI-2 Campaign: Part 1—Development of a New Retrieval Algorithm" was analyzed and used as a reference study for this work.

3.4.1 Reference Study

The CINDI-2 campaign (Cabauw Inter-comparison campaign of Nitrogen Dioxide measuring Instruments-2) was held in Cabauw (52°N, 5°E), the Netherlands, during September 2016. The main objective of the campaign was the inter-calibration of remote sensing instruments using the DOAS technique to monitor air quality and validate satellite observations. More than 40 instruments operated by 30 groups participated in the campaign, including MAX-DOAS instruments, in situ systems and balloon sondes. Measurements made by the MPIC tube MAX-DOAS instrument during the period from 12 to 28 September, 2016, were used in the study, given in table 6.

To begin the sensitive study, baseline settings were developed for QDOAS analysis. FWHM was changed to 0.7 (depending on instrument) and locally generated calibration file was used. Fitting interval of 320-340nm (from the CINDI-2 study) and four tropospheric ozone cross sections (TO_3, TO_3A, PO_3B and PO_3D) besides the ring cross-section were added in the O_3 analysis window.

3.4.2 Optimization of Polynomial Order

Keeping the aforementioned parameters constant, polynomial order was changed from none to 8, applying no Intensity Offset (based on reference study). The process was repeated for data from three different (bright summer) days to determine the polynomial order generating the lowest error. On comparison of RMS and error for each setting, it was found that two polynomial orders, 3 and 4, provided optimum results with minimum errors. Both these values were used in the next step of the sensitive study, i.e. determining the ozone fitting interval. At the end of the sensitive study, all optimized parameters were input in QDOAS and polynomial order was again changed from none to 8 to recheck its suitability. Figure 11 compares the analysis results for a single spectrum recorded during the afternoon at the elevation viewing angle of 45 degrees on 8th August 2018.

Polynomial Order: None

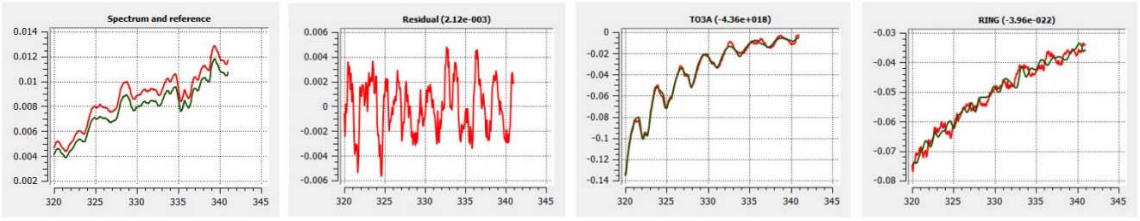

Polynomial Order: 0

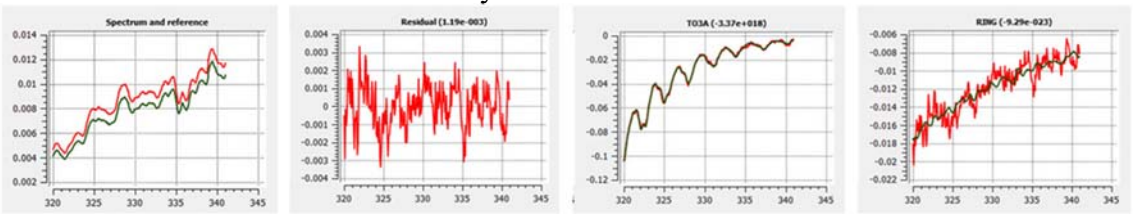

Polynomial Order: 1

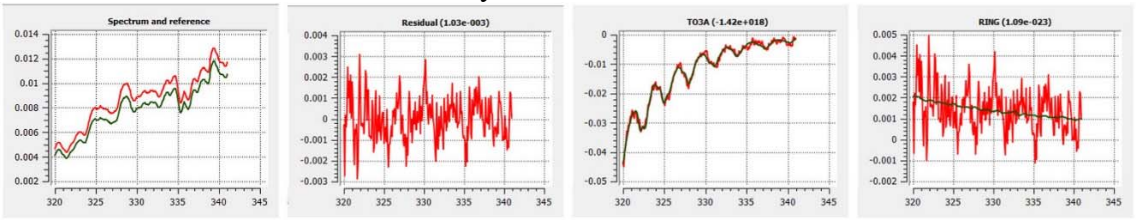

Polynomial order: 2

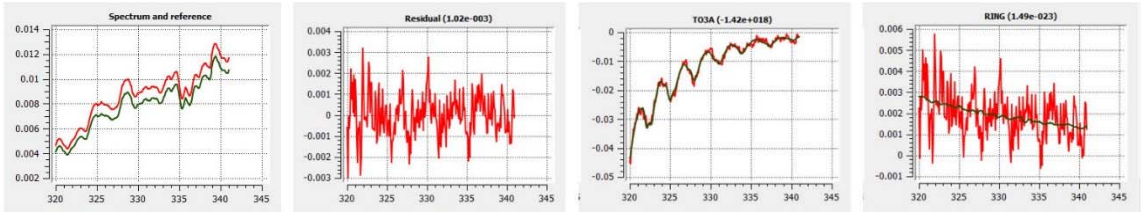

Polynomial order: 3

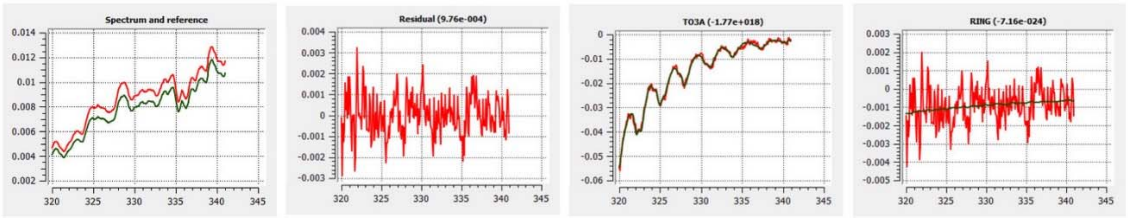

Polynomial order: 4

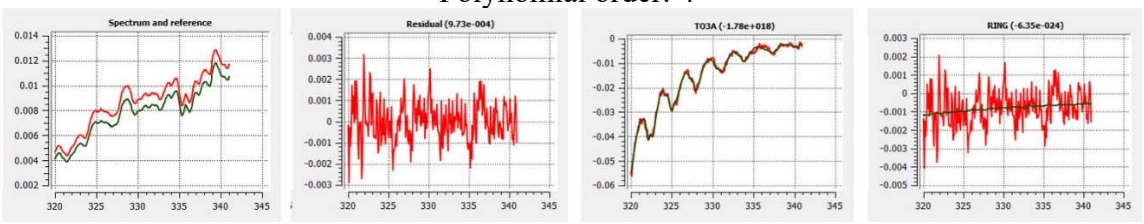

Polynomial order: 5

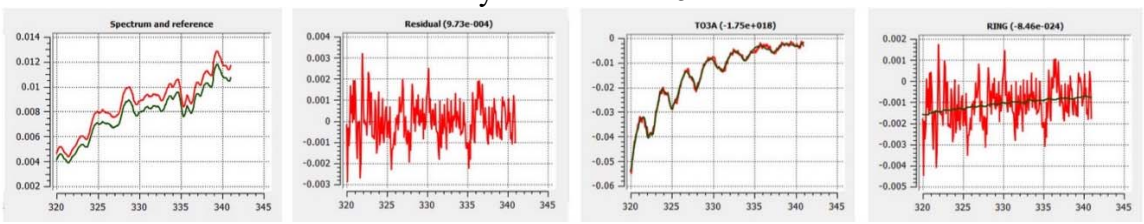

Polynomial order: 6

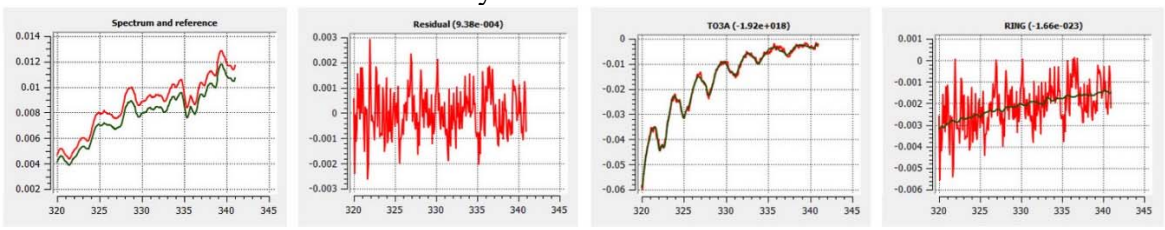

Polynomial order: 7

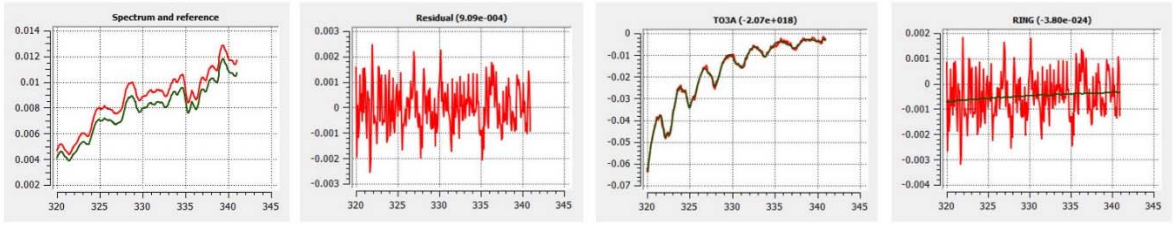

Polynomial order: 8

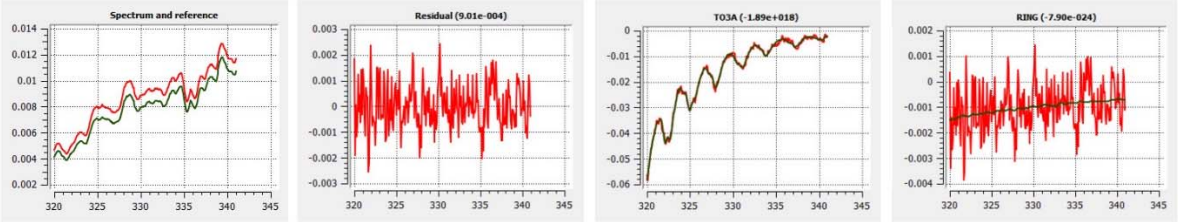

Figure 1 Polynomial order (none to 8) applied on optimal settings

3.4.3 Optimization of Ozone Fitting Interval

In order to determine the optimum fitting interval for ozone retrieval, the lowest limit (320nm) and the highest limit (345nm) were identified for ozone, based on literature. Three different (bright summer) days were selected and QDOAS analysis were run multiple times with different fitting intervals, each interval in turn run with polynomial order 3 and 4 separately. Figure 12 shows comparison of various fitting intervals using MS Excel. Fitting interval of 320-341nm and polynomial order of 4 were identified as being optimum.

3.4.4 Optimization of Trace Gas Cross Sections

Trace gas retrieval from MAX-DOAS is impacted by all other trace gases with absorption in the same spectral window. All such trace gas cross-sections must be used in QDOAS to filter out their impact on the target gas. During the sensitive study, five trace gases that share the ozone's spectral window were considered. The five trace gases and the six corresponding cross-sections (two cross sections calculated at different temperatures were used for O_4, both treated separately) are given in table 7.

One day (sunny) was selected from each month of the year 2018 and all possible combinations of cross-sections were used separately to analyze the data for each day. Cross sections used in CINDI-2 study were also among the list of 11 combinations identified. Results were tabulated in MS Excel and three parameters were calculated for each retrieval:

1. **Quadratic Sum of dSCDs**

Quadratic Sum of dSCDs = SQRT ($dSCD_a$^2+$dSCD_b$^2…+$dSCD_n$^2)

Where $dSCD_{a..n}$ represent the dSCDs of the cross sections used in the analysis.

2. **Quadratic Sum of Errors**

Quadratic Sum of Errors = SQRT ($error_a$^2+$error_b$^2…+$error_n$^2)

Where $error_{a..n}$ represent the errors of the cross sections used in the analysis.

3. **% Uncertainty in Ozone Retrieval**

% Uncertainty = (Quadratic Sum of Errors/Quadratic Sum of dSCDs)*100

The three parameters were compared for each setting to determine the setting with the lowest quadratic sum of errors and the least % uncertainty. RMS values were also analyzed and final settings were determined. The cross sections which resulted in the lowest error and least % uncertainty are:

1. O_4_Hermans
2. HCHO_297K_Meller
3. NO_2_298K_VanDaele
4. BrO_223K_Fleischmann

Figure 13 shows the comparison of various cross sections using MS Excel.

3.5 Analysis of O_3

The parameters determined by the sensitive study were input in the O_3 Analysis window in the QDOAS software. Figures 14 shows the O_3 analysis window properties whereas figures 15-16 show the QDOAS project properties and output tab for dSCD generation. The analysis was performed on all retrieved spectra and O_3 dSCDs were generated in ASCII format file. Differential Slant column density (dSCD) is the total density of the

given gas, O_3, measured along the entire light path reaching the instrument, and not the total column density right above the instrument. For this reason, in order to measure the true column density of ozone directly above the instrument, slant column densities are converted into vertical column densities using the air mass factor, explained in detail in the subsequent section.

3.5.1 Conversion of dSCDs into VCDs

To obtain Vertical Column Densities from Slant Column Densities, the ASCII files generated by the QDOAS software are run in excel. First; all negative values of TO_3A are filtered out and removed as these represent errors in the spectra. Second; all the outlying values of RMS are removed to smoothen the data. Next, Air Mass Factor (AMF) is used to convert the slant column densities into vertical column densities. Air mass factor is defined as the ratio of dSCDs and VCDs, calculated using the following equation:

$$\mathbf{AMF = 1 / \sin(2*3.14*EVA/360)}$$

(Where EVA = Elevation viewing angle)

AMF, once calculated, is used for generating VCDs using the following equation:

$$\mathbf{VCD = O_3.SlCol(TO_3A) / (AMF-1)}$$

Finally; the VCDs for Elevation Viewing Angle 30 are filtered out and the VCDs generated at all other angles are discarded. Figure 17 shows comparison between dSCDs and VCDs.

3.5.2 Generation of Daily Diurnal Values

Diurnal values represent the fluctuations that occur from hour to hour within a day. These values present a picture of how the column densities of the measured trace gas i.e. O_3 changes throughout the day. Diurnals are calculated from the VCD files, using an algorithm

developed by the software Python. Figure 18 shows the daily diurnal values for the month of January 2018, calculated using python from the VCDs.

3.5.3 Generation of Ozone Trends

Daily diurnal values of ozone were calculated for data spanning 4 years from March 2015 to March 2019. After removing outlying values and error files, various trends were generated to explain it graphically. These trends include:

1. Daily Averages of tropospheric ozone from March 2015 to March 2019.
2. Diurnal trend of tropospheric ozone from March 2015 to March 2019.
3. Seasonal Diurnal trends for the four seasons;
    - Pre-monsoon extending from March to May
    - Monsoon extending from June to September
    - Post-Monsoon extending from October to November
    - Winter extending from December to February
4. Weekly trend of tropospheric ozone from March 2015 to March 2019.
5. Monthly trend of tropospheric ozone from March 2015 to March 2019.
6. Seasonal trends, i.e. average of all the months of each season from March 2015 to March 2019.

3.5.4 Comparisons and Correlations

Various comparisons and correlations were generated to determine the factors that impact the column densities of tropospheric ozone and to what extent. The parameters considered during this study were:

1. Normalized Difference Vegetation Index (NDVI)
2. Temperature
3. Global Horizontal Irradiance (GHI)

3.5.5 Determining compliance with WHO standard

The 8-hour average standard for ozone is given as mixing ratios (parts per billion) by the World Health Organization (WHO standard guidelines). For deriving mixing ratios from column densities, boundary layer height is an important factor. For the purposes of this study, boundary layer height was taken as constant at 1500m. The National Environmental Quality standard for tropospheric ozone developed by Pak-EPA could not be used because it only provides one-hour average standard for ozone.

3.6 Validation of MAX-DOAS measurements

In order to validate the MAX-DOAS data collected at ground level at IESE-NUST, it was compared against data obtained from the combined product of MLS/OMI instruments for the time period from March 2015 to December 2017. Raster data obtained from the satellite product was converted and geo-referenced in ARCMAP 10.3. Shape file for Islamabad was superimposed over the map and point location of IESE NUST identified to obtain monthly column densities in molecules/cm^2 at the site of the MAX-DOAS instrument. Monthly average values were obtained from the satellite data and compared with MAX-DOAS measurements.

Chapter 4

RESULTS AND DISCUSSION

4.1 Retrieval of Tropospheric O_3 column densities from MAX-DOAS

Tropospheric ozone VCDs retrieved from MAX-DOAS instrument at the study site were analyzed to generate various trends, comparisons and correlations. The study identified the

trend of tropospheric ozone during the whole study period and identified the impacts of various external factors (Temperature, GHI etc.) on observed tropospheric ozone column densities.

4.1.1 Daily Average of Tropospheric Ozone

Daily average Tropospheric Ozone column densities were calculated for the four-year period and plotted against date to identify the temporal trend. Standard deviation was also calculated for each day to determine the extent to which the column densities of ozone vary from one hour to another during the same day. The trend of daily average tropospheric ozone is presented in figure 19.

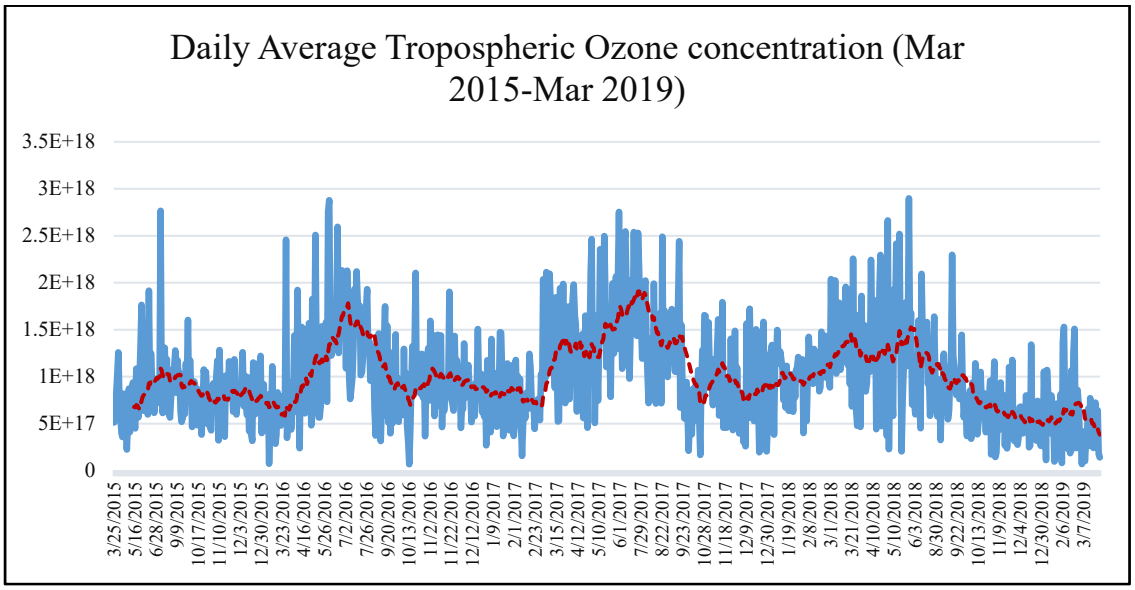

Figure 2 Daily Average Tropospheric Ozone column densities at study site (March 2015-March 2019)

Tropospheric Ozone column at the study site begins to rise during the month of March as weather starts to get warmer, reaching peak levels during the three hottest months of the year, May, June and July. During the month of August as the weather starts to cool, tropospheric ozone column densities at the study site begin to decrease, reaching minimum

levels in December/January. The trendline shows rising ozone levels during the warmer months of the year.

4.1.2 Diurnal Cycle of Tropospheric Ozone

Figure 20 shows the diurnal cycle for the study period from March 2015 to March 2019. Tropospheric Ozone column densities depends upon two factors; precursor emissions and sunlight intensity. Lowest levels are observed during the first hour i.e. 6:00 am – 6:59 am due to weak sunlight. Highest column densities are observed at peak traffic hours and around noon time. It is further observed that standard deviation remains nearly similar for all hours.

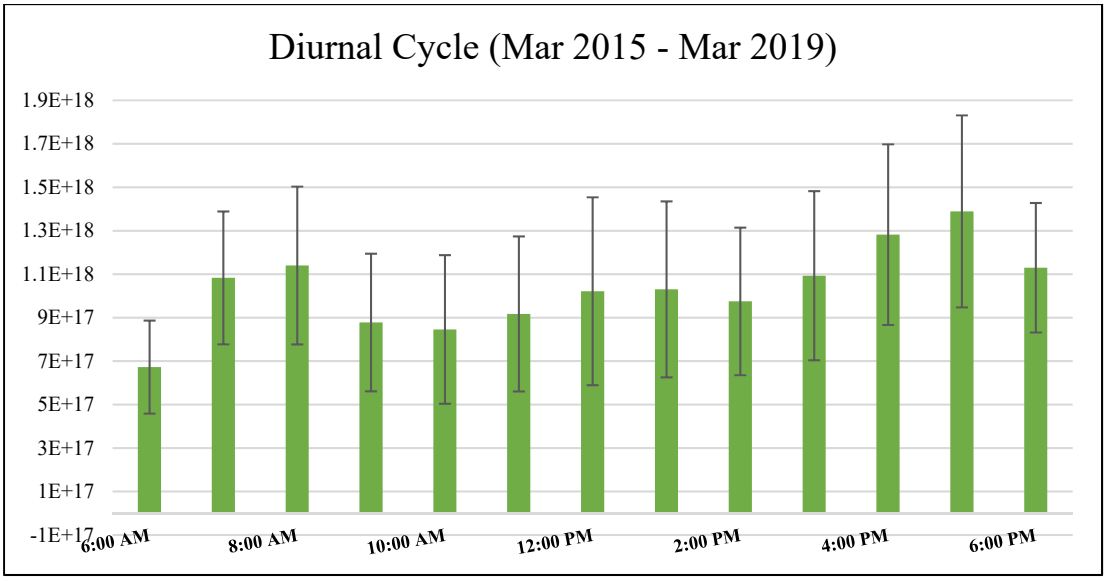

Figure 3 Diurnal Cycle of Tropospheric Ozone (March 2015 - March 2019)

4.1.3 Seasonal Diurnal Cycles of Tropospheric Ozone

The relationship between meteorological conditions and generation of tropospheric ozone column has been explored by various studies over the years. In order to isolate the impact of weather conditions on production of tropospheric ozone, diurnal cycles were generated separately for all four seasons i.e. Pre-Monsoon, Monsoon, Post-Monsoon and Winter as presented below.

Pre-Monsoon

Figure 21 shows the diurnal cycle for the 3 months of pre-monsoon; March, April and May, from March 2015 to March 2019. Lowest levels are observed during the first hour i.e. 6:00 am – 6:59 am due to weak sunlight. Highest column densities are observed at peak traffic hours i.e. 7:00 am – 8:59 am and 4:00 pm – 6:59 pm. Ozone column densities measured around noon are noticeably lower than ones observed at peak traffic hours, enforcing the role of sunlight intensity in tropospheric ozone creation.

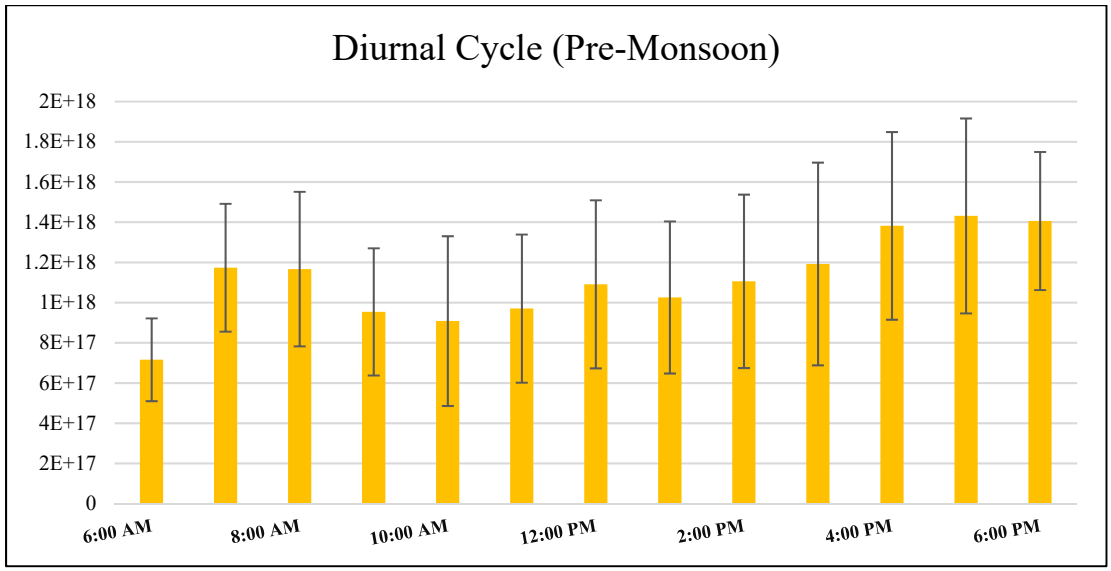

Figure 4 Diurnal Cycle of Tropospheric Ozone (Pre-Monsoon Season)

Monsoon

Figure 22 shows the diurnal cycle for the 4 months of monsoon; June, July, August and September, from June 2015 to September 2018. High column densities are observed during the peak traffic hours in morning (7:am – 8:59 am) and evening (4:00 pm – 5:59 pm). However, the highest column densities are observed around noon (12:00 pm – 12:59 pm),

suggesting that strong sunlight and high temperature result in the domination of ozone creation reactions.

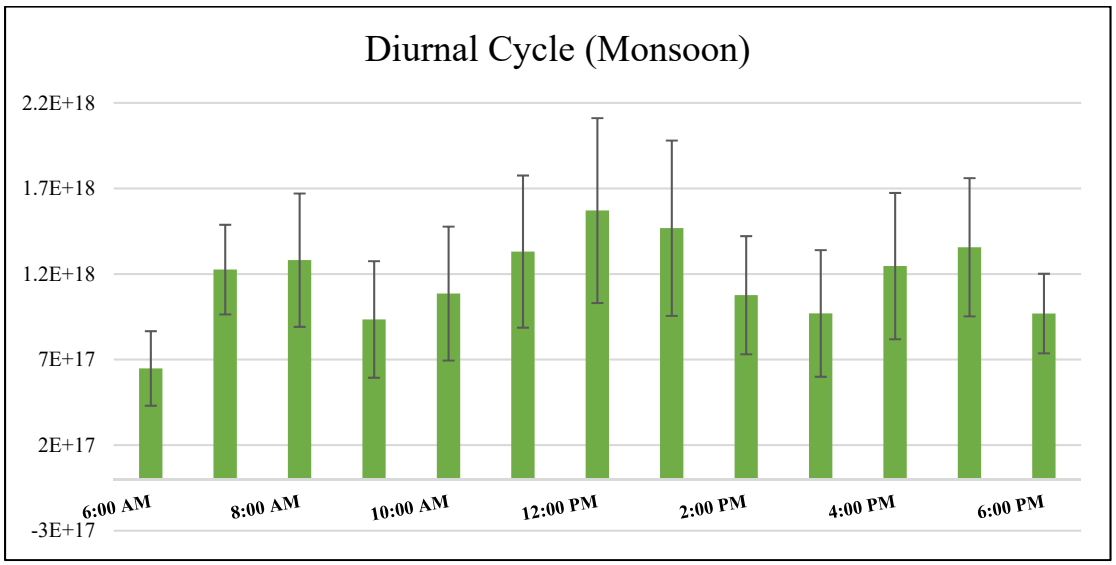

Figure 5 Diurnal Cycle of Tropospheric Ozone (Monsoon Season)

Post Monsoon

Figure 23 shows the diurnal cycle for the 2 months of post-monsoon; October and November. Significant drops in ozone column densities have been observed as the temperature lowers over the months. Furthermore, daylight hours shrink from 6:00 am – 6:59 pm to 7:00 am – 4:59 pm as days become shorter. Highest column densities are observed during peak traffic hours. Lowest column densities are observed around noon as the balance between ozone production and ozone destruction cycles shifts due to weak sunlight and precursor emissions become the limiting factor.

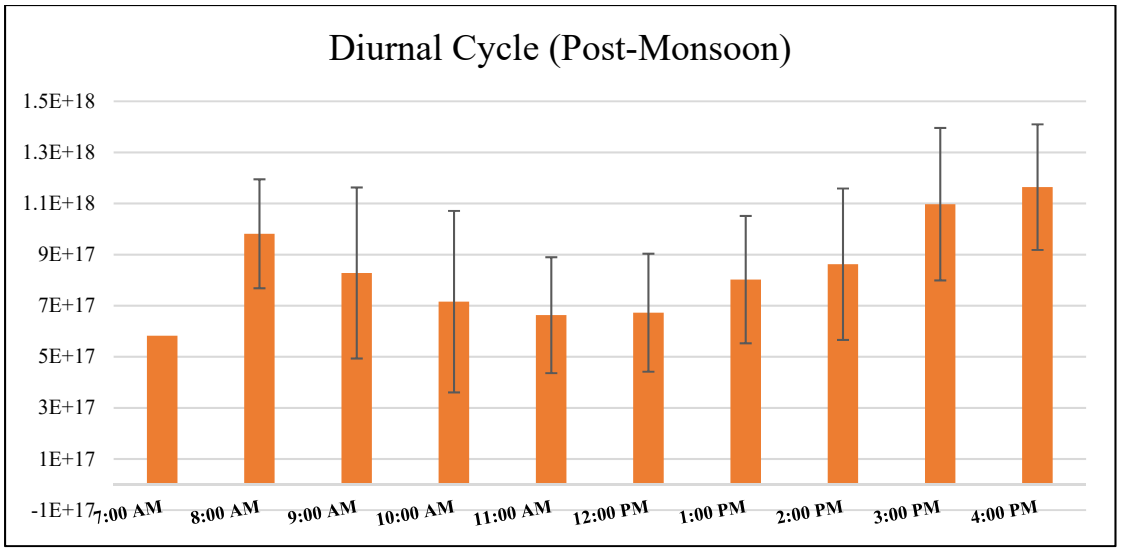

Figure 6 Diurnal Cycle of Tropospheric Ozone (Post - Monsoon Season)

Winter

Figure 24 shows the diurnal cycle for the 3 months of winter; December, January and February. Highest column densities are observed during peak traffic hours and lowest column densities are observed in the morning. Ozone production lifts slightly around noon but precursor emissions remain the limiting factor.

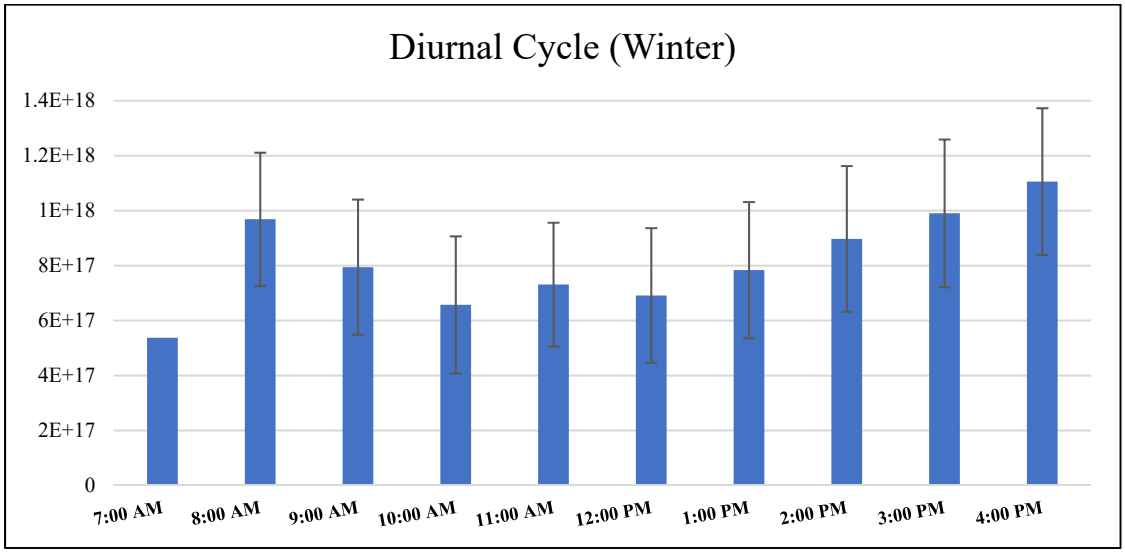

Figure 7 Diurnal Cycle of Tropospheric Ozone (Winter Season)

4.1.4 Weekly Cycle of Tropospheric Ozone

Figure 25 shows the weekly cycle of tropospheric ozone averaged from March 2015 to March 2019. Ozone column remains nearly constant throughout the entire week. Ozone production depends upon sunlight and precursor emissions. The low distance between the study site and the Kashmir Highway as well as settlements surrounding the university on all sides ensure the availability of precursor emissions.

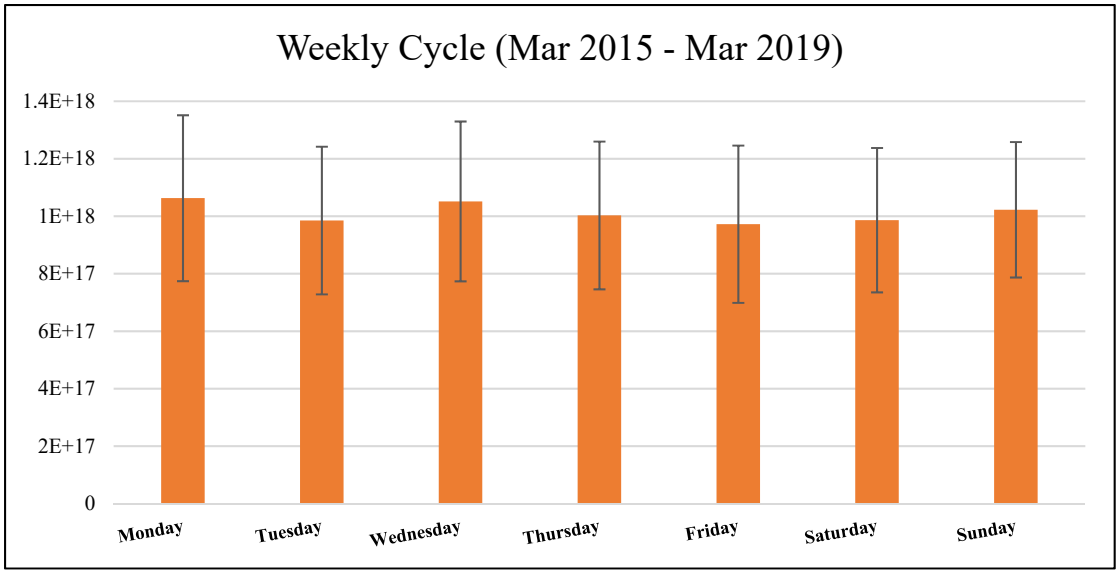

Figure 8 Weekly Cycle of Tropospheric Ozone (March 2015 - March 2019)

4.1.5 Monthly Cycle of Tropospheric Ozone

Figure 26 shows the monthly cycle of ozone for the study period, March 2015 – March 2019. Column densities recorded each month have been averaged over the four years, running the cycle from March to February. Tropospheric ozone column densities at study site rise with temperature, reaching their peak in the month of July. The hottest month of the year also has the lowest standard deviation i.e. high column densities were recorded across all the months of July during the study period.

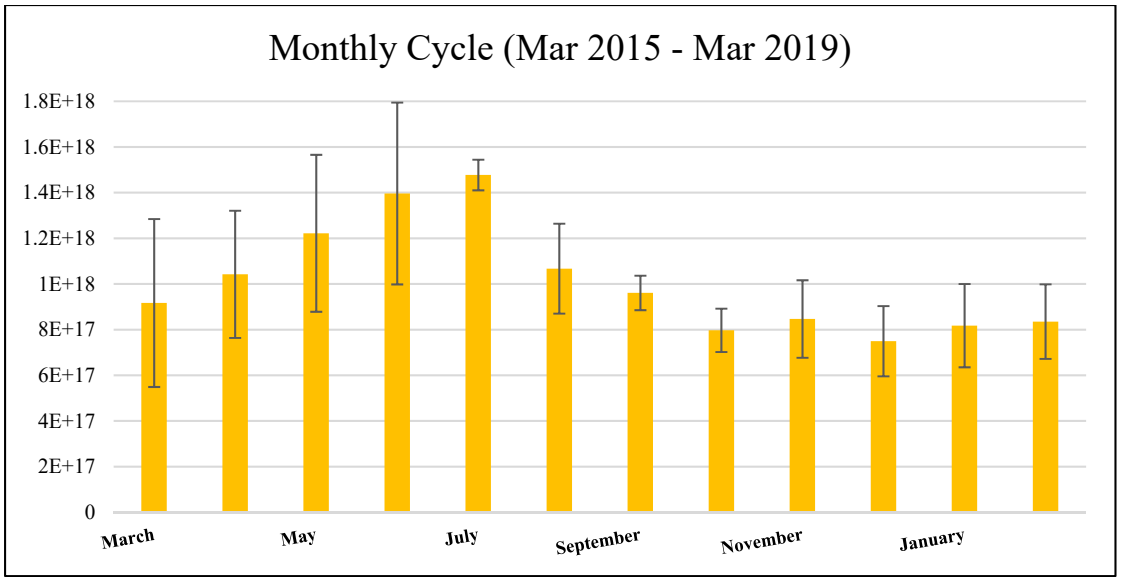

Figure 9 Monthly Cycle of Tropospheric Ozone (March 2015 - March 2019)

Tropospheric ozone displays a sharp downward trend following the month of July and column densities remain low during the colder months of the year. Some fluctuation is inevitably observed during these months and it may be attributed to precursor emission levels especially during winter months when higher amounts of fuel are consumed for heating purposes and due to lower boundary layer height.

Figure 27 represents all 46 months for which data was collected during the study. The graph depicts how ozone column densities change over the years for the same months. Highest concentrations were observed during the months of June and July. It may be noted that no usable data was available for the 3 months of Jan 2016, Feb 2016 and July 2018. The instrument, during these months, was employed in field monitoring of various trace gases across the country.

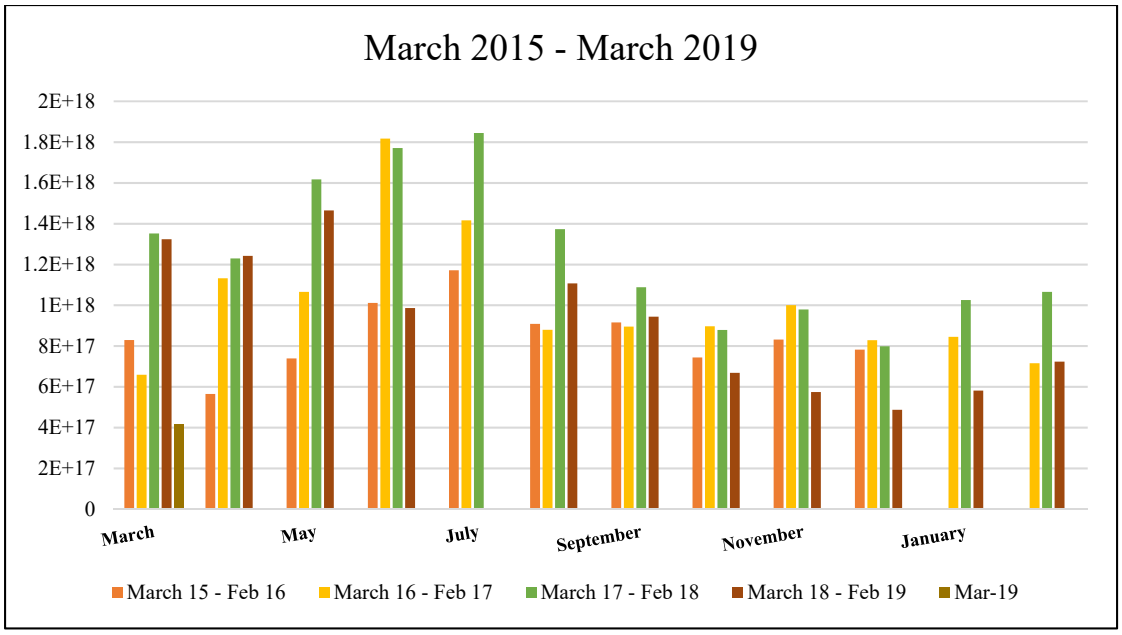

Figure 10 Monthly Variations observed in Tropospheric Ozone (March 2015 - March 2019)

4.1.6 Seasonal Cycle of Tropospheric Ozone

Figure 28 shows the seasonal cycle of tropospheric ozone across the study period. It is noted that tropospheric ozone levels are high during pre-monsoon and monsoon seasons, corresponding to the presence of strong sunlight. Ozone levels drop significantly in the colder post-monsoon months, corresponding to dimmer sunlight and little or no availability of Biogenic VOCs emissions.

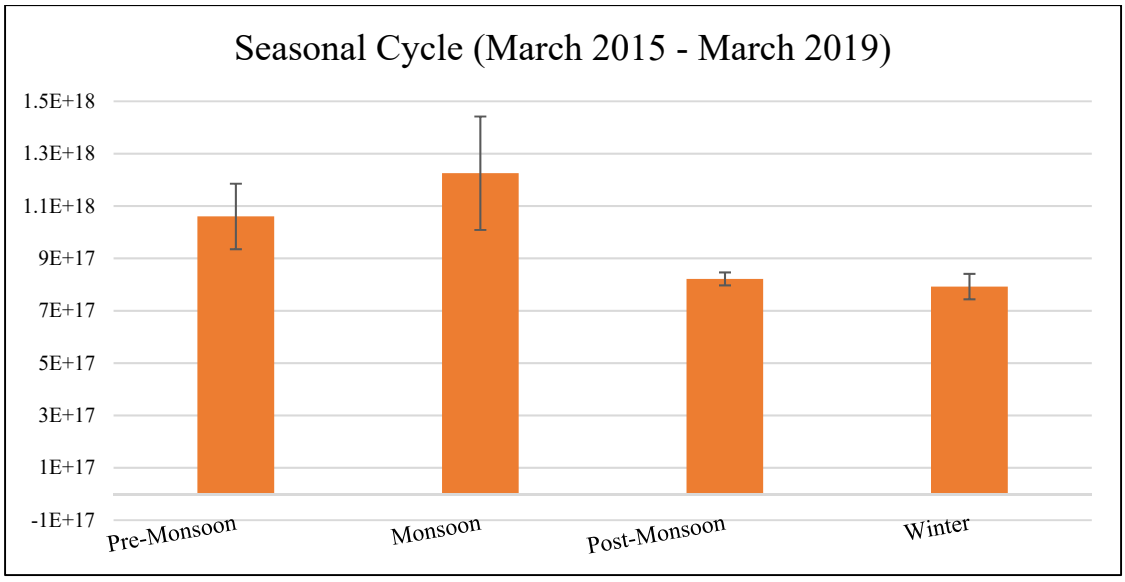

Figure 11 Seasonal Cycle of Tropospheric Ozone (March 2015 - March 2019)

4.2 Comparisons and Correlations of Tropospheric Ozone

To understand the impact of meteorological conditions and vegetation cover on the presence of tropospheric ozone at the study site, various parameters were studied and comparisons and correlations with ozone column densities were developed. These Correlations are:

1. Temperature and Tropospheric Ozone
2. Global Horizontal Irradiance (GHI) and Tropospheric Ozone
3. Normalized Difference Vegetation Index (NDVI) and Tropospheric Ozone

4.2.1 Comparison between Temperature and Tropospheric Ozone

To understand the impact of temperature on the production and distribution of tropospheric ozone, average monthly temperature values were compared with average monthly MAX-DOAS measurements, shown in figure 29. Temperature data was obtained from ESMAP

Tier-1 Meteorological Station at USPCASE, NUST. Ozone column densities increase with rising temperatures, though significant variations are observed.

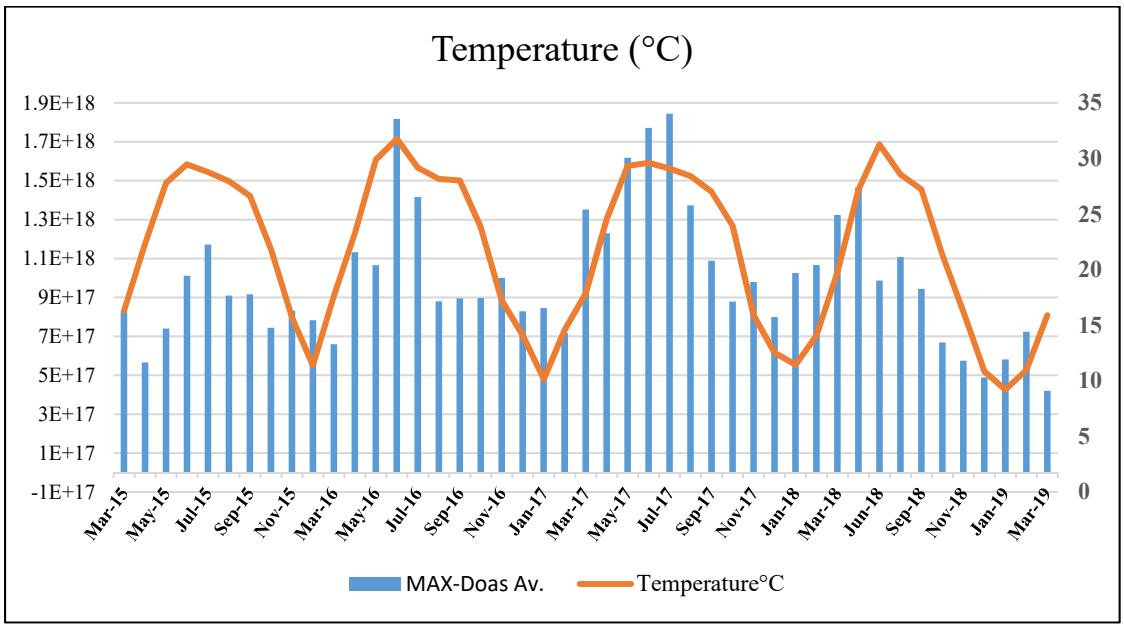

Figure 12 Comparison between Temperature and MAX-DOAS observations of tropospheric ozone column

The correlation between MAX-DOAS observations of tropospheric ozone and temperature is presented in figure 30. The variables are directly related with a moderate correlation i.e. Pearson value r = 0.579. The correlation establishes partial dependence of ozone production on temperature, suggesting that other factors exert a significant influence on the production of tropospheric ozone.

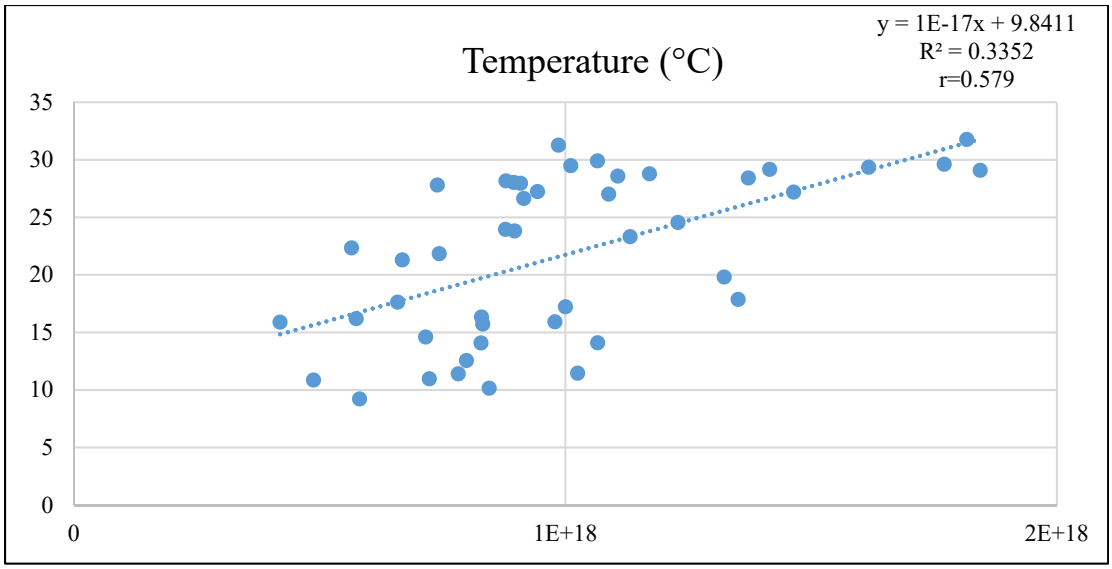

Figure 13 Correlation between Temperature and MAX-DOAS observations of tropospheric ozone column

4.2.2 Comparison between GHI and Tropospheric Ozone

Monthly GHI data was obtained from ESMAP Tier1 Meteorological Station at USPCASE, NUST and compared with monthly tropospheric ozone column densities measured using MAX-DOAS instrument at the study site. The comparison is presented in figure 31. GHI gives an accurate depiction of sunlight intensity at a given point and time. Ozone column densities show increase with increase in Global Horizontal Irradiance, though significant variations are observed, suggesting the dependence of ozone production on other factors such as pre-cursor emissions.

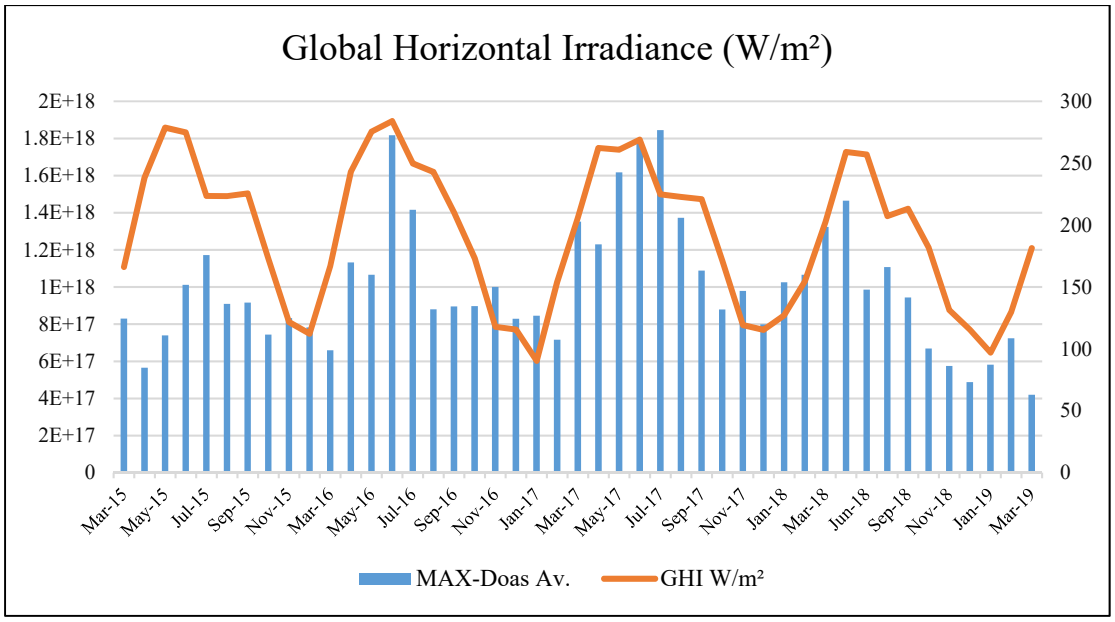

Figure 14 Comparison between GHI and MAX-DOAS observations of tropospheric ozone column

The correlation between MAX-DOAS observations of tropospheric ozone and global horizontal irradiance is presented in figure 32. The variables are directly related with a moderate correlation i.e. Pearson value r = 0.565, establishing partial dependence of tropospheric ozone production on GHI.

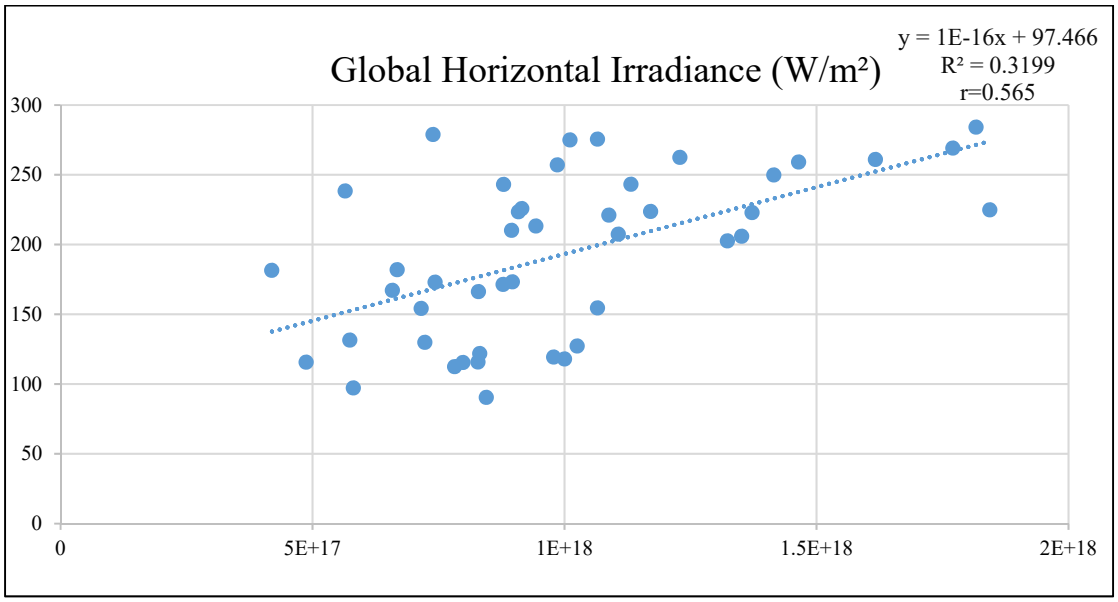

Figure 15 Correlation between GHI and MAX-DOAS observations of tropospheric ozone column

4.2.3 Comparison between NDVI and Tropospheric Ozone

To study the impact of vegetation on tropospheric ozone column, comparison and correlation between NDVI and ozone column was performed. It is a measurement of the reflectivity of plants expressed as the ratio of near-infrared reflectivity (NIR) minus red reflectivity (VIS) over NIR plus VIS, calculated using the formula:

NDVI -= NIR-VIS / NIR+VIS

To calculate NDVI for the green area surrounding the instrument's location, site images were taken from the LANDSAT 8 satellite and atmospheric correction was applied on the images using QGIS3. Following atmospheric correction, NDVI was calculated in ArcMAP using the visible red band and near-infrared band extracted from the LANDSAT images. NDVI values below 0.3 and the observations for the corresponding months were removed from the data in favor of accuracy. The resulting graph presented in figure 33 shows the lack of a significant relation between NDVI and tropospheric ozone. This is affirmed by the correlation between MAX-DOAS observations of tropospheric ozone and NDVI presented in figure 34. The variables showed an insignificant correlation i.e. Pearson value $r = 0.07$.

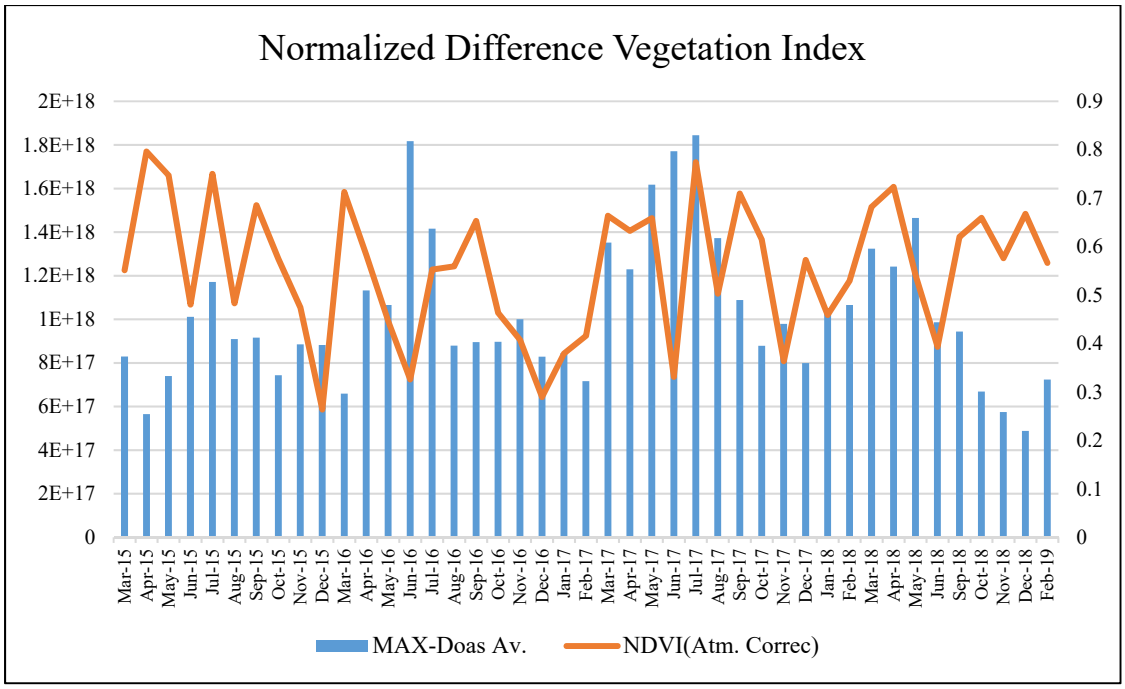

Figure 16 Comparison between NDVI and MAX-DOAS observations of tropospheric ozone column

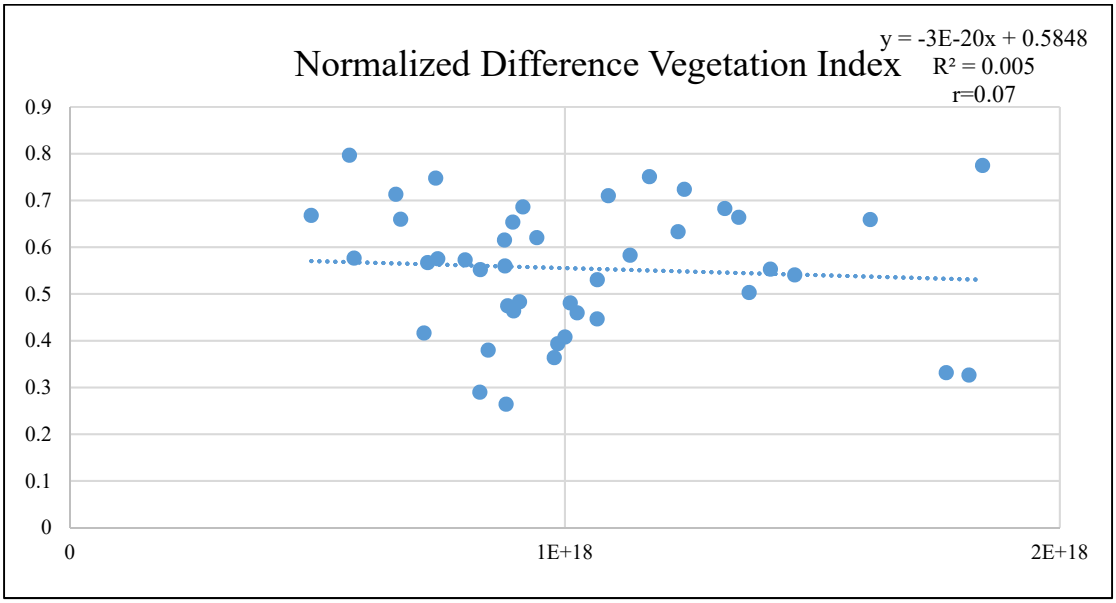

Figure 17 Correlation between NDVI and MAX-DOAS observations of tropospheric ozone column

4.3 Conversion of Ozone column into Ozone mixing ratios

Various air pollution standards have been developed at national and international levels which set threshold limits for different air pollutants. In the case of ozone, Pak-EPA has set the limit for 1-hour average of ozone, which is set at 130 µg/m³. However, MAX-DOAS observations have been made over a longer timescale 6:00 am – 6:59 pm, thus the WHO standard for 8-hour average of ozone, set at 100 µg/m³ was used for compliance monitoring. The various steps involved in compliance monitoring are presented in the following sub-sections.

4.3.1 Conversion of column densities into ppb values

MAX-DOAS measurements are made on the scale of molecules per cm^2 whereas the standards are given in µg/m³. For comparison, both values were converted to a uniform scale i.e. ppb. The Conversion factor for ozone, developed by the UK Air Quality Archive for reporting data to the WHO, determined at 25°C and 1013mb is:

1 ppb of ozone = 1.96 µg m^{-3} of ozone

WHO standard for 8-hour average of ozone = 100 µg/m³

100 µg/m³ = 100/1.96 ppb = 51.02 ppb

In order to convert the MAX-DOAS observations in molecules/cm^2 into ppb values, it was necessary to consider the air pressure above the instrument site and the boundary layer height. Air pressure remains constant at a certain point, in this case it was taken as 1190. Boundary layer height was kept constant at 1500m.

4.3.2 Calculation of Daily Ozone ppb values

Figure 35 shows the various steps involved in obtaining ppb values of tropospheric ozone from MAX-DOAS measurements. A series of conversions were applied on the measured values using parameters such as boundary layer height and air pressure. The ppb values obtained were placed side by side with the ppb value of the WHO standard in order to compare and determine compliance.

38	Date and Day	Daily Average	BLH	O3 mol/cm3	P_1000m	ρ_Mol/m3	ρ_Mol/cm3	O3/Air Ratio	O3/ppbv	WHO (8Hr)
39	3/25/2015	5.14139E+17	1500	3.42759E+11	1190	2.47366E+25	2.47366E+19	1.38564E-08	13.86	51.02
40	3/26/2015	6.1722E+17	1500	4.1148E+11	1190	2.47366E+25	2.47366E+19	1.66345E-08	16.63	51.02
41	3/27/2015	8.26873E+17	1500	5.51249E+11	1190	2.47366E+25	2.47366E+19	2.22848E-08	22.28	51.02
42	3/28/2015	1.01612E+18	1500	6.77414E+11	1190	2.47366E+25	2.47366E+19	2.73851E-08	27.39	51.02
43	3/29/2015	1.25737E+18	1500	8.38249E+11	1190	2.47366E+25	2.47366E+19	3.3887E-08	33.89	51.02
44	3/30/2015	7.45298E+17	1500	4.96865E+11	1190	2.47366E+25	2.47366E+19	2.00863E-08	20.09	51.02
45	4/9/2015	5.6498E+17	1500	3.76653E+11	1190	2.47366E+25	2.47366E+19	1.52266E-08	15.23	51.02
46	4/10/2015	3.99258E+17	1500	2.66172E+11	1190	2.47366E+25	2.47366E+19	1.07603E-08	10.76	51.02
47	4/11/2015	3.5842E+17	1500	2.38947E+11	1190	2.47366E+25	2.47366E+19	9.65966E-09	9.66	51.02
48	4/14/2015	8.18247E+17	1500	5.45498E+11	1190	2.47366E+25	2.47366E+19	2.20523E-08	22.05	51.02
49	4/15/2015	7.23151E+17	1500	4.82101E+11	1190	2.47366E+25	2.47366E+19	1.94894E-08	19.49	51.02
50	4/17/2015	5.74471E+17	1500	3.82981E+11	1190	2.47366E+25	2.47366E+19	1.54824E-08	15.48	51.02
51	4/21/2015	2.24793E+17	1500	1.49862E+11	1190	2.47366E+25	2.47366E+19	6.05833E-09	6.06	51.02
52	4/22/2015	4.7876E+17	1500	3.19173E+11	1190	2.47366E+25	2.47366E+19	1.29029E-08	12.90	51.02
53	4/24/2015	8.71948E+17	1500	5.81299E+11	1190	2.47366E+25	2.47366E+19	2.34996E-08	23.50	51.02
54	4/25/2015	4.11205E+17	1500	2.74137E+11	1190	2.47366E+25	2.47366E+19	1.10822E-08	11.08	51.02
55	4/26/2015	7.92396E+17	1500	5.28264E+11	1190	2.47366E+25	2.47366E+19	2.13556E-08	21.36	51.02
56	5/13/2015	8.95588E+17	1500	5.97059E+11	1190	2.47366E+25	2.47366E+19	2.41367E-08	24.14	51.02

Figure 18 Determination of ozone ppb values

Figure 36 shows the trend of tropospheric ozone mixing ratios over the study period. Highest ppb values were observed during the warmer months, corresponding to the observed columns of tropospheric ozone.

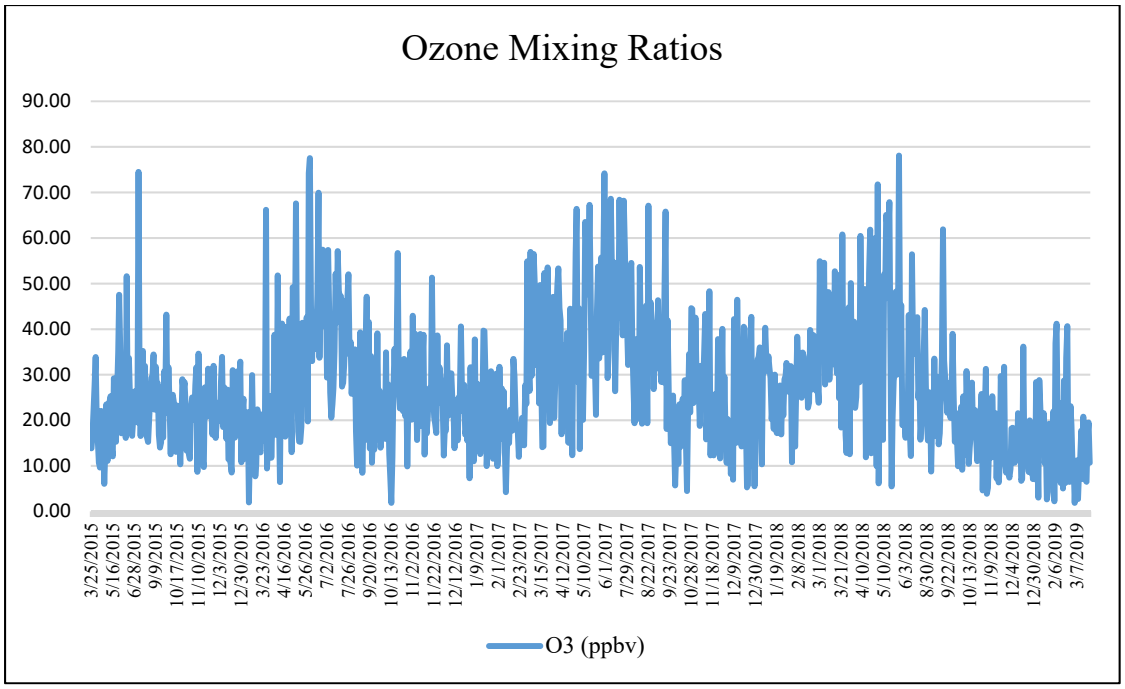

Figure 19 Trend of ozone ppb values across the study period (March 2015 - March 2019)

4.4 Comparison with the WHO standard

In the final step, ppb values of ozone across the entire study period March 2015 – March 2019 were compared against the WHO standard for ozone i.e. 51.02 to determine whether or not the observed ozone values were within WHO limits. Figure 37 shows the comparison between MAX-DOAS observations and the standard set by the World Health Organization. It may be noted that MAX-DOAS observations are within the limit set down by the World Health Organization during most of the study days. Significant non-compliance is observed during various days in pre-monsoon and monsoon seasons when ozone production is high due to high temperature and intense sunlight.

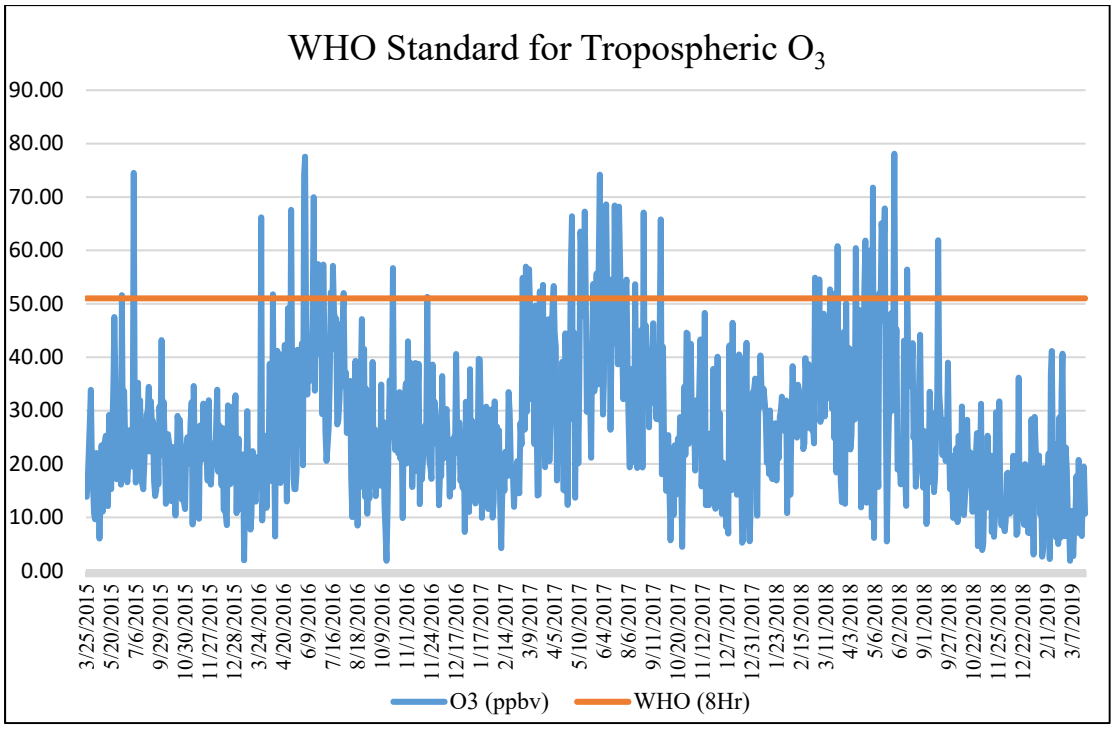

Figure 20 Comparison of MAX-DOAS observations with the WHO standard for Tropospheric Ozone

4.5 Validation of MAX-DOAS observations using MLS/OMI satellite data

To validate MAX-DOAS observations, MLS/OMI satellite data was retrieved through GIOVANNI. Monthly column densities of tropospheric ozone measured by the MLS/OMI satellite were retrieved using ARCMAP 10.3. Since the satellite passes over the study area sometime between 1:00 pm and 2:00 pm, the diurnals for that hour alone were averaged across the entire month and compared against the satellite data. OMI satellite data was available for the time between March 2015 – December 2017 (Data for 2018 and 2019 was unavailable at the time of analysis). The trend presented in figure 38 was generated by monthly data averaged across the 34 months.

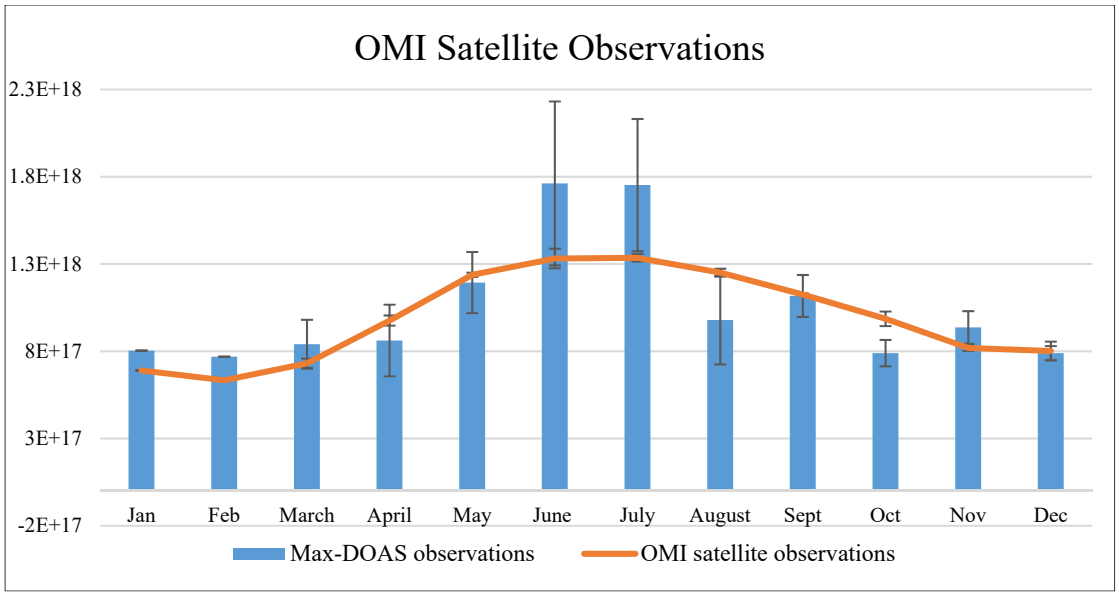

Figure 21 Comparison between OMI satellite observations and MAX-DOAS observations

The two sets of observations follow a similar trend across the year. However, significant underestimation by OMI satellite is observed during the two hottest months of June and July. This may be due to several factors such as cloud cover, aerosol and water vapor content in the atmosphere which significantly obscure the ground level trace gases.

The two sets of observations show a direct relation with a strong correlation i.e. Pearson value r = 0.801, presented in figure 39. It may be noted that the ground-based stationary MAX-DOAS measurements are in good agreement with the satellite measurements made by the OMI satellite.

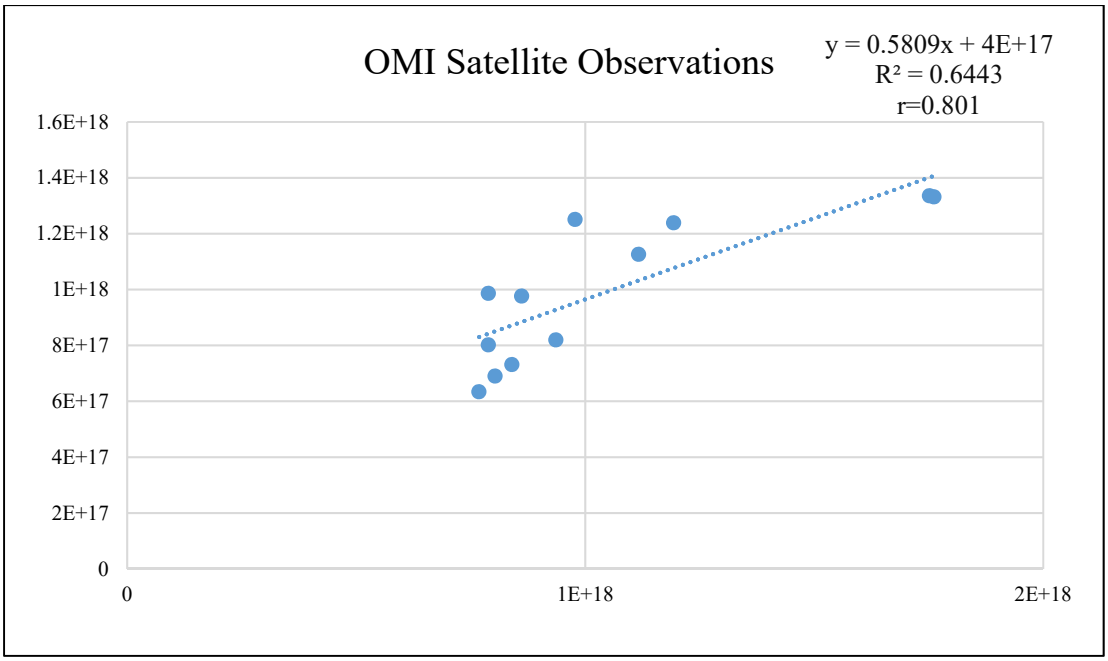

Figure 22 Correlation between OMI satellite observations and MAX-DOAS observations

Chapter 5

CONCLUSION AND RECOMMENDATIONS

5.1 Conclusion

The MAX-DOAS observations performed were carried out in order to identify tropospheric ozone levels in the study area. The study covered a four-year period from March 2015 – March 2019 and discovered changes in tropospheric ozone column across the period. The MAX-DOAS observations were compared with temperature and global horizontal irradiance to determine the role of weather conditions. The measurements have also been compared against satellite observations made by MLS/OMI satellite as it passes over the study site.

Following are the optimum conditions identified during this study for retrieval of tropospheric ozone column densities from the MAX-DOAS instrument:

Following are the conclusions drawn from the study:

- Increase in tropospheric ozone column were observed around noon as well as around peak traffic hours. This indicates a strong correlation between production of tropospheric ozone and sunlight as well as between tropospheric ozone and traffic emissions from the neighboring region.
- Higher tropospheric ozone was observed during the warm seasons i.e. pre-monsoon and monsoon as compared to the cold seasons i.e. post-monsoon and winter.

- Tropospheric ozone values show moderate correlations with temperature (r=0.579) and global horizontal irradiance (r=0.56), indicating that weather conditions might have an impact on the production of tropospheric ozone.
- MAX-DOAS observations show a strong correlation with combined MLS/OMI satellite observations (r=0.80), validating the settings used to retrieve MAX-DOAS tropospheric ozone column densities.